Investigations of non-visible features in archaeological sites: testing aerial remote sensing with UAV in Pompeii

*Virtual Archaeology Review*, **17**(34): 1–25, 2026
https://doi.org/10.4995/var.2024.24163


Received: June 18, 2025
Accepted: September 1, 2025

# INVESTIGATIONS OF NON-VISIBLE FEATURES IN ARCHAEOLOGICAL SITES: TESTING AERIAL REMOTE SENSING WITH UAV IN POMPEII

## *INVESTIGACIÓN DE ELEMENTOS NO VISIBLES EN SITIOS ARQUEOLÓGICOS: EVALUACIÓN DE LA TELEDETECCIÓN AÉREA CON UAV EN POMPEYA*

Valentina Santoro*, Zhiguo Wu, Giacomo Patrucco, Antonia Spanò

Lab G4CH, Department of Architecture and Design (DAD), Politecnico di Torino, Viale Mattioli, 39, 10125, Torino, Italy.
valentina.santoro@polito.it; zhiguo.wu@polito.it; giacomo.patrucco@polito.it; antonia.spano@polito.it

**Highlights:**

- This research highlights unmanned aerial vehicle (UAV) multispectral imagery as a versatile, cost-effective tool for non-invasive archaeological prospection within a complementary, multi-disciplinary strategy.
- The study assesses a commercial multispectral sensor (DJI Mavic 3M), in the historically significant context of Pompeii, integrating prior archaeological excavations and geophysical surveys.
- By analysing UAV spectral index maps, known and additional anomalies were identified; a confidence map showing anomaly frequency facilitated the comparison with geophysical and excavation data.

**Abstract:**

The study described below aims to confirm the potential of UAV-based multispectral imagery as a flexible and cost-effective tool to detect possible buried archaeological structures, expanding upon previous approaches based on satellite or traditional airborne data. In parallel, the authors investigate the role of such imagery within a conjectured workflow that incorporates multispectral analysis as a preliminary, extensive, and non-invasive step in archaeological prospection strategies. The study evaluates the performance of a commercial sensor and analyses spectral signatures by generating index maps within the significant context of *Iulia Felix Praedia* in Pompeii (Italy). A significant opportunity was the possibility of acquiring multispectral data in the *hortus* area, previously investigated through non-invasive geophysical surveys and archaeological excavations. The UAV photogrammetric flight, as well as the subsequent analyses, focused on the visual interpretation and geolocated examination of vegetation and soil index maps, accurately selected among those available, considering the UAV-acquired band dataset. This approach enhanced the feature of the complex *hortus* environment, where natural elements alternate with numerous man-made structures. These analyses led to the detection of anomalies, consistent with those previously identified by the aforementioned investigations, alongside additional anomalies distributed across the study area. The detected anomalies were further analysed and synthesised; this involved generating a confidence map based on the frequency of the anomaly occurrence across the analysed index maps. The consistency between detected anomalies and previous investigations' results underlines the potential for continued research on processing multispectral data captured by UAVs. Thanks to such data, a valuable alternative to satellite imagery was provided, due to their much higher spatial resolution, enabling rapid and cost-effective campaigns to plan more targeted geophysical and archaeological investigations. The findings also validate the hypothesised workflow involving the use of multispectral imagery as a preliminary, extensive, and non-invasive tool to define excavation areas' perimeters and, subsequently, guide targeted analyses.

**Keywords:** multispectral data; aerial remote sensing; unmanned aerial vehicle (UAV); spectral indices; index maps; archaeological investigations

**Resumen:**

El estudio descrito abajo tiene como objetivo confirmar el potencial de la imagen multiespectral basada en vehículo aéreo no tripulado (UAV) como una herramienta flexible y rentable para detectar estructuras arqueológicas enterradas, ampliando enfoques previos basados en datos satelitales o aerotransportados tradicionales. Paralelamente, se investiga el papel de esta tecnología dentro de un flujo de trabajo que incorpora el análisis multiespectral como un paso preliminar, extenso y no invasivo, en estrategias de prospección arqueológica. Se evalúa el rendimiento de un sensor comercial y se analizan firmas espectrales mediante la generación de mapas índice en el contexto de *Iulia Felix Praedia*, en Pompeya (Italia). La oportunidad clave fue la adquisición de datos multiespectrales en el área del hortus, previamente investigada mediante estudios geofísicos no invasivos y excavaciones arqueológicas. El vuelo fotogramétrico con UAV, así como los análisis posteriores, se centraron en la interpretación visual y el examen geolocalizado de mapas índice de vegetación y suelo, seleccionados entre las bandas adquiridas por el UAV. Este enfoque permitió mejorar la caracterización del complejo entorno del hortus, donde elementos naturales alternan con estructuras hechas por el hombre. Estos análisis detectaron anomalías consistentes con las identificadas en

* Corresponding author: Valentina Santoro, valentina.santoro@polito.it

investigaciones anteriores, además de nuevas anomalías distribuidas por toda el área estudiada. Una síntesis adicional generó un mapa de confianza basado en la frecuencia de aparición de anomalías en los mapas índice analizados. La concordancia entre anomalías detectadas y resultados previos subraya el potencial para continuar investigando el procesamiento de datos multiespectrales capturados por UAV. Estos datos ofrecen una alternativa valiosa a la imagen satelital debido a su mayor resolución espacial, permitiendo campañas rápidas y rentables para planificar investigaciones geofísicas y arqueológicas más específicas. Los resultados también validan el flujo de trabajo que usa la imagen multiespectral como herramienta preliminar, extensa y no invasiva, para definir perímetros de excavación y guiar análisis focalizados.

**Palabras clave:** datos multiespectrales; teledetección aérea; vehículo aéreo no tripulado (UAV); índices espectrales; mapas de índices; investigaciones arqueológicas

## 1. Introduction

Archaeological research is considered one of the most interdisciplinary fields of study. It is no coincidence that remote sensing technologies from airborne and spaceborne sensors are widely used and well-documented in literature for the identification of new sites, the study of archaeological landscapes, and the monitoring of historical areas for their conservation (Cigna & Tapete, 2021). The development of new sensors and innovations in analysis techniques, combined with data fusion and the proven benefit of integrating multiple methods, significantly enhances our knowledge of archaeological sites, enabling more accurate investigations (Cebrián, Hortelano, Ortiz, & Vallés, 2024; Masini et al., 2023). These factors shape the future directions for developing new strategies and methods in the field of remote sensing applied to archaeology.

Among the most promising techniques in recent years —also thanks to sensor miniaturisation and the spread of Unmanned Aircraft System (UAS)— is the application of multispectral imagery acquired from Unmanned Aerial Vehicles (UAVs). Similarly, to well-established satellite-based approaches, this technique enables the detection of spectral anomalies at different wavelengths across the surveyed surface. These anomalies are often linked to variations in material composition or to specific surface conditions —such as differences in growth or nutrient availability in the case of vegetation— typically resulting in what are known as crop marks. In archaeological contexts, these anomalies are frequently associated with the presence of buried structures that affect the properties of the overlying crop or soil (Gojda & Hejcman, 2012).

It is also important to highlight that the Faro Convention (Council of Europe, 2005) underlines the value of cultural heritage and its potential as a resource for sustainable development, promoting a broader understanding of heritage and its relationship with communities by encouraging the active participation of citizens and developing cultural identities. This has an outstanding impact on the sphere of archaeological heritage. These imperatives not only raise the threshold of sharing and disseminating research results but also indirectly push us to evaluate preventive archaeology with ever more significant commitment. In this sense, there is a growing need to leverage techniques that enable a more precise identification of the areas where the excavation –often long, costly, yet indispensable– can provide higher levels of information and knowledge development.

The paper is structured to provide, in the following Sections (1.1 and 1.2), the research objectives in relation to relevant works developed in the field of remote sensing methods, including multispectral investigations, as well as a description of the case study–an *insula* of Pompeii– along with the schematic framework of the archaeological research program that involved this site. Subsequently, Section 2 (Materials and Methods) reports in detail the photogrammetric data acquisitions from systems in both the visible and non-visible ranges of the electromagnetic spectrum, including the generation of orthophotos derived from different spectral bands and the calculation of index maps. Section 3 (Results) describes the outcomes and possible interpretations of the index maps anomalies, while in Section 4 (Discussion) the results of aerial remote sensing with UAV are evaluated and compared with the interpretations of the geophysical anomalies and the results derived from the consequent stratigraphic investigations. Finally, in the conclusions (Section 5), some considerations are provided on both the results of the investigations using multispectral imagery from UAV and the future development prospects of the adopted methods.

### 1.1. Aims of the research and related works

Recently, aerial remote sensing using UAV has emerged as a powerful tool, enabling the possibility of carrying out image analyses to assess ground conditions and potentially detect submerged structures, exploiting the very large scale of mapping enabled by UAS technology. This integration allows for highly detailed analysis results (Santoro, Patrucco, Lingua, & Spanò, 2023; Verhoeven, Smet, Poelman, & Vermeulen, 2009). One of the most interesting aspects that emerged in the present research is connected to the opportunity of acquiring multispectral data using UAVs in an archaeological area where a season of integrated research had just concluded, enabling the possibility of integrating geophysical prospections with archaeological excavation tests that validated the hypotheses for identifying submerged structures. It is worth considering this opportunity within the broader context of remote sensing methodologies for cultural and landscape heritage, which have been evolving for a long time (Luo et al., 2019). These methodologies aim at different goals depending on the use of different sensors –both active (range-based) and passive (image-based)– as well as the platforms from which they operate, offering several distance-based approaches in the spaceborne, airborne and terrestrial sectors.

Archaeological traces resulting from human activities on the territory have been defined as landscape engineering, referring to the ways in which ancient communities modified and shaped during their settlement processes. These modifications represent a significant challenge for remote sensing aimed at detecting and highlighting them (Traviglia & Torsello, 2017). Investigations aimed at detecting landscape

patterns have primarily focused on using space sensors and analyses based on data fusion techniques. These approaches combine high spatial resolution imagery with the spectral richness of multispectral satellite datasets, along with various strategies to enhance the identification of land features (Masini & Lasaponara, 2006).

Currently, the unprecedented spread of remote sensing data in the satellite sector has greatly increased its availability, particularly thanks to the open-access availability of certain missions, such as Sentinel 2. However, a crucial challenge in the field of heritage monitoring still depends on the size of the Ground Sampling Distance (GSD), whose effectiveness can be enhanced, as recently demonstrated, through super-resolution algorithms that improve application feedback (Lanaras, Bioucas-Dias, Galliani, Baltsavias, & Schindler, 2018).

The great attention previously devoted to advancing automation in geoinformation analyses and processing, has recently been extended to the field of Cultural Heritage (CH) and, within it, to the study of archaeological landscapes. However, many studies that pursue automation, also state that the delay or difficulty of affirmation in the field of heritage is struggling to spread due to a consolidated distrust that assigns to the study of heritage a necessary interpretation of the operator (Traviglia & Torsello, 2017). While innovations in the use of machine learning and deep learning techniques have been significantly developed for the classification of both 3D and 2D datasets, proposals for automation in the CH field have also emerged, starting from data derived from both active (Cappellazzo, Patrucco, Sammartano, Baldo, & Spanò, 2024) and passive sensors (Sonnemann et al., 2017).

Traditional satellite remote sensing methods, based on photointerpretation and manual vectorisation for mapping, were gradually supplemented from the second half of the 20$^{th}$ century by more advanced techniques, such as image classification, index creation, and automatic polygon extraction (Costa, Benevides, Marcelino, & Caetano, 2020; Davis, 2021; Machala, Honzova, & Klimánek, 2015). Initially applied in satellite-based remote sensing, these developments have significantly enhanced the detection and investigation of archaeological features. In the last decade, these methods were integrated with more advanced technologies, including the recent development of UAS platforms, which have proven particularly valuable in the documentation of archaeological sites. The term UAS refers to the entire flight system, comprising the aircraft, control stations, and data link whereas UAV refers solely to the aerial component (Chao, Cao, & Chen, 2010). UAVs can be categorised both by their operational parameters —such as maximum flight altitude, range, and distance from the take-off point (Watts, Ambrosia, & Hinkley, 2012)— and by their physical characteristics, including aerodynamic configuration and size. In this regard, the most common types are fixed-wing and rotary-wing systems. The former requires a runway for take-off and landing and is characterised by long endurance, high wind resistance, and the ability to fly at high speeds. On the other hand, rotary-wing UAV are equipped with multiple rotors and rotating wings, which provide the advantages of hovering capability and high manoeuvrability (Gupta, Ghonge, & Jawandhiya, 2013). Given their ability to carry both active and passive sensors, UAV platforms offer high productivity and a favourable cost–benefit ratio, providing detailed and adaptable insights due to their scale of analysis and ease of integration with terrestrial 3D surveying methods —thus enabling a multiscale approach.

Surely, among the passive sensors, the adoption of optical cameras opened up to UAV visible (VIS) photogrammetry, which has become an efficient tool in archaeology, ensuring rich radiometric information and has a high capacity to generate 3D models of the excavation and upstanding building structures by combining nadir and oblique imagery (Aicardi et al., 2016; Sammartano, Chiabrando, & Spanò, 2020; Sauerbier & Eisenbeiss, 2010). The study of site microtopography meets the investigation needs of numerous application fields (Johnson et al., 2014), including landscapes and archaeological research. In these contexts, both the contextualisation of archaeological evidence within the natural landscape and the extraction of highly accurate profiles provide valuable insights for interpretation (Nikolakopoulos, Soura, Koukouvelas, & Argyropoulos, 2017).

Thanks to the possibility of capturing information in the non-visible range of the electromagnetic spectrum, which allows for the study of the behaviour of different materials identified by their spectral signatures (Schaepman et al., 2009), multispectral sensors –among the domain of passive sensors- equipped on UASs have recently proven particularly effective in various fields, such as precision agriculture and forestry (Belcore, Pittarello, Lingua, & Lonati, 2021; Kapari et al., 2025; Zhang et al., 2025). These sensors increase the scale and improve the level of detail compared to similar analyses carried out using data acquired from more distant sensors. However, there are few studies focused on enhancing the interest in using these technologies for the knowledge, monitoring and valorisation of archaeological heritage (Fassbinder et al., 2025; Fiz et al., 2022; Hill, Laugier, & Casana, 2020; Moriarty, Cowley, Wade, & Nichol, 2019). Most of these studies aim to detect anomalies in order to verify the correlation between the presence of cropmarks –detectable through the use of multispectral indices– and potential submerged structures. These investigations typically rely on data obtained from the acquisition of different infrared wavelengths to detect these cropmarks (Calleja et al., 2018; Casana & Ferwerda, 2024; Ronchi, Limongiello, & Barba, 2020), since analysing this portion of the electromagnetic spectrum is particularly effective for the detection of anomalies (primarily associated with vegetation health). Very often, these methods are complemented by the integrated study enabled by the generation of Digital Surface Models/Digital Terrain Models (DSMs/DTMs), computed through the integration of both image-based and range-based sensors, which are predominantly based on LiDAR technology and are highly effective in providing accurate geometric data. In many scenarios, these surface models highly enhance the readability of the detected anomalies in archaeological sites and landscapes (Ronchi et al., 2020). It is also interesting to note the more frequent integration of these active sensors with optical imagery to supplement spectral data. Recently, the advent of active Multispectral and Hyperspectral LiDAR (MSL/HSL) systems, which operate at multiple wavelengths, is revolutionising the simultaneous acquisition of height and intensity information (Takhtkeshha, Mandlburger, Remondino, & Hyyppä, 2024). In recent years, within the framework of

studies carried out in the non-visible range of the electromagnetic spectrum, there have also been numerous research experiences in which the acquisition of Thermal Infrared (TIR) imagery has been evaluated for this type of investigation (Agudo, Pajas, Pérez-Cabello, Redón, & Lebrón, 2018; Hollesen, Jepsen, & Harmsen, 2023; Patrucco, Cortese, Giulio Tonolo, & Spanò, 2020; Salgado Carmona, Quirós, Mayoral, & Charro, 2020). This non-destructive and contactless approach has proven particularly effective in the framework of multispectral monitoring, allowing for the identification of buried structures and archaeological evidences by exploiting the different emissivity –and consequently, the different temperature– of the material composing the submerged structures compared to that of the surrounding soil. These studies evidence that the interest in this type of technology is driven by the need, on one hand, to ensure sustainable and efficient methods to support archaeological investigations while defining excavation areas' perimeters, and on the other hand, to develop non-invasive and non-destructive methods coherent with the intrinsic fragility of CH. Building on this framework, the present study aims to assess the feasibility and effectiveness UAV-based multispectral imaging as a high-resolution, cost-effective, and rapid tool for detecting surface-level spectral anomalies, as indirect indicators of subsurface potential archaeological buried structures. The objective is to propose a hierarchical strategy for site investigation in which multispectral imaging is a preliminary, scalable screening approach and a first layer of interpretation that can guide and optimise more targeted analyses. In particular, the method can help in the prioritisation of specific zones, to narrow down areas of interest and inform the planning of more specific geophysical surveys or excavations. The case study conducted at the site of the *Praedia* of *Iulia Felix* in Pompeii serves to test the applicability of this approach in an urban archaeological context.

## 1.2. Case study and previous investigations

The case study of the present contribution is the *Praedia* of *Iulia Felix* in *Regio* II of Pompeii ancient city (Figure 1), located near the vital area used for public entertainment including the amphitheatre and the *Palestra Grande*. The term *praedia* refers to a property or plot of land. In the insula of the *Praedia* of *Iulia Felix* (*insula* II 4), a variety of settlement typologies coexist, ranging from a conventional atrium house corresponding to the residential nucleus in the south-west sector of the *insula*, to a suburban villa conceived with a relevant park, a swimming pool with nymphaeum, sumptuous reception halls and rooms overlooking nature. Additionally, there is a commercial sector, including the so-called public *balnea* and *tabernae* of different sizes (Anguissola & Olivito, 2022a). PRAEDIA is also the acronym for the research project Pompeian Residential Architecture: Environmental, Digital, Interdisciplinary Archive, which includes integrated studies on domestic constructions in the *Regio* II sector of Pompeii. The project aims to investigate archaic phases preceding the 79 AD eruption, while also encompassing the early studies and excavations from the 18th century to present-day initiatives aimed at enhancing the use of the archaeological site (Anguissola & Olivito, 2022a).

The archaeological research suggests that the *Praedia* was built between the late 1st century BC and the early 1st century AD (Anguissola & Olivito, 2022c). In particular, the research has focused on the vast *hortus*, which, as previous stratigraphic excavations tests from the 1990s (Parslow, 1988) indicate the possibility of shedding light on the frequentation and organisation of the city before the Samnite age, extending into the late Republican ages. On the basis of the excavation tests that had revealed wall structures referable to water channels, the PRAEDIA project has planned to carry out non-destructive geophysical investigations in 2016 and 2018, through 3 different methods —Magnetometric


(a) (b)

**Figure 1**: (a) The *Praedia* of *Iulia Felix* (highlighted in red) in the context of the southeast quadrant of Pompeii, precisely the area of *Regio* II pertaining to a peripheral but lively city area, with the amphitheatre and the *Palestra Grande*. Orthophoto from the visible data acquisition performed in 2023. (b) Map highlighting the areas investigated using Ground Penetrating Radar (GPR) (orange), Vertical Magnetic Gradient (VMG) (yellow), and those subjected to archaeological excavation (light blue).

survey (MAG), Ground Penetrating Radar (GPR), Frequency-Domain Electromagnetics Method (FDEM) (Marchetti, Materni, Sapia, & Urbini, 2022; Urbini et al., 2021)— as it is currently a usual research standard to compare the results of different methods to investigate possible submerged structures and direct targeted stratigraphic excavations (Marchetti et al., 2022; Urbini et al., 2021). Considering that the geophysical investigations as a whole have revealed numerous anomalies further to the excavation tests of the 1990s, at a depth of 40 cm and 80 cm, confirming the presence of a 16th-century canal already known in literature and defined as Count *Sarno*'s channel (Paone & Rispoli, 2011), in addition to possible walls of probable Archaic Age, in 2019 and 2020, the PRAEDIA program has foreseen the stratigraphic investigation in numerous excavation tests distributed in the *hortus*, to intercept both the excavations of the 1990s and the anomalies identified by the geophysical investigations. Building on these investigations, the geomatics elaborations presented in the following section are aimed at exploring the results of the aerial remote sensing with UAS. They are intended to assess whether the anomalies identified from the spectral signatures of the terrain in different index maps correspond to previously documented features, using the results of geophysical surveys and excavation tests as ground truth data for validation. Further details, including descriptions and georeferenced maps and images of these analyses, are provided in the *Discussion* section.

## 2. Materials and methods

The combined acquisitions in both the visible and non-visible range of the electromagnetic spectrum using UAS photogrammetry, described in this section, aimed at investigating the south-eastern quadrant of *Regio* II of Pompeii. This area includes both the *Palestra Grande* and the region between the *Palestra Grande* and the amphitheatre. The latter area was the subject of recent stratigraphic excavations, which highlighted the presence of submerged structures related to water storage and probable canalisations. While the multispectral analyses focus on the *hortus* of the *Iulia Felix Praedia*, parallel research, concerns the evidence found in *Palestra Grande* and surrounding areas.

From a technical 3D metric survey perspective, the Pompeii areas present some critical challenges: the regions under analysis are covered by vegetation, including tall trees (Fig. 2), and are open to tourists, which complicates geomatics activities.

In accordance with the Italian Civil Aviation Law, UAS flights have been carried out by licensed pilots both before and after the archaeological park's opening to the public. These regulatory constraints significantly affected the planning of multispectral data acquisition, as they imposed limitations on flight scheduling —an aspect that is particularly critical for this type of survey and will be further discussed in Section 2.2.

Another important observation concerns the type of photogrammetric flights. While certain technical strategies, such as repetition at different times of the day, will be discussed later, it is essential to highlight that modern photogrammetric practice easily supports the use of the so-called direct photogrammetry. This method allows for the direct determination of the coordinates of the image projection centres during the flight, enabling the bundle adjustment solution without the use of GCPs measured through traditional topographic method. However, this solution was avoided because, in the *Praedia* (as well as in other *insulae* of the *Regio II*) another 3D integrated survey was carried out. This involved performing terrestrial LiDAR-based (Light Detection and Ranging) 3D surveying using TLS (Terrestrial Laser Scanning) approach, along with SLAM-based (Simultaneous Localisation and Mapping) mobile scanning. Thus, the integration of different (visible) aerial and terrestrial 3D technologies results can be optimised, increasing the accuracy of each technique's results with the support of control points. The terrestrial activities are not discussed in this manuscript, but they enable to understand the reason for the use of a topographic control network, the details of which will be addressed in the next section. A second reason that imposes the use of a topographical control network is related to the *Grande Pompei* project, developed by the Archaeological Pompeii Park in the 1990s. This program aimed to implement refined and effective conservation and enhancement activities for the site. It also established a dense network of topographic vertices, encouraging archaeological research groups working in Pompeii from around the world to use this reference system for mapping and sharing purposes.


**Figure 2:** Aerial image of the Praedia of Iulia Felix, highlighting the presence of trees and vegetation that affect flight planning and cast shadows over the area to be surveyed.

### 2.1. Topographic control network and different reference systems

Based on the situation outlined in the previous section, the 3D metric survey of *Regio* II started by establishing a topographic control network consisting of 6 topographic vertices. This preliminary step enabled the management of 3D spatial data within a single reference system.

The topographic control network was surveyed using the Global Navigation Satellite System (GNSS) technique, adopting the international standard UTM WGS 84 (Zone 33N) reference system. Each vertex, distributed in different *insulae*, was measured in static mode, as illustrated in Fig. 3. The vertices coordinated were processed and adjusted using a least squares compensation procedure, involving data from three permanent stations (Napoli, Avellino, Torre del Greco). This approach allowed us to obtain a good average accuracy, with standard deviations of approximately 3-4 mm for the planimetric coordinates and approximately 8-10 mm for the heights, as observable in Table 1.

(a)

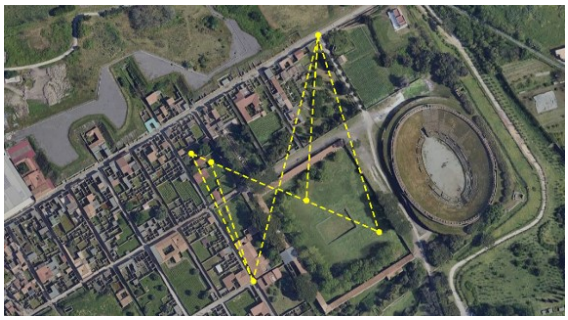

(b)

**Figure 3**: (a) Set up of GNSS receiver on the vertex located in the Palestra; (b) scheme of the topographic control network in the *Regio* II, Pompeii.

**Table 1**: Standard Deviation of topographic control network coordinates enabling the assessment of a very good accuracy of vertices' positions.

| *Vertices* | *SD LAT WGS84 [m]* | *SD LONG WGS84 [m]* | *SD Altitude [m]* |
|---|---|---|---|
| 005 | 0.003 | 0.002 | 0.009 |
| 017 | 0.002 | 0.002 | 0.008 |
| 100 | 0.003 | 0.002 | 0.010 |
| 200 | 0.002 | 0.002 | 0.008 |
| 400 | 0.003 | 0.003 | 0.010 |

The goal of obtaining the vertices' coordinates —and consequently all mapping results— in two different reference systems was achieved by measuring two vertices of known coordinates from the existing Pompeii topographical network. These vertices (005, in *Via dell'Abbondanza*, and 017, in *Via Nocera*; these two vertices were chosen from those located at the north-east and the south-west extremes of the topographic network) are two of the six points belonging to the topographical control network established for the survey described in this research. The first reference system is the universally adopted UTM WGS 84 (Zone 33N in southern Italy), while the second one corresponds to the *Grande Pompei* topographic network, which is based on the former Italian cartographic reference system, namely Gauss Boaga. The coordinates of the GCPs used to orient the data acquired from the photogrammetric flights have been measured using Real-Time Kinematic (RTK) GNSS technique, achieving centimetre-level accuracy. Their spatial distribution within the area can be observed in Fig. 4.

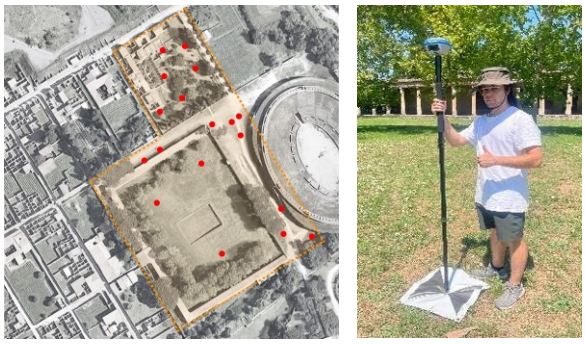

(a) (b)

**Figure 4**: (a) GCPs scheme evenly distributed in the area of interest adopted for the photogrammetric flights; (b) a sample of GNSS/RTK measurements.

## 2.2. UAV visible and multispectral data: acquisition and processing

During the survey campaign, several photogrammetric flights were carried out with the aim of acquiring images both in the visible range of the electromagnetic spectrum and in the non-visible range, namely, in the Red Edge (RE) and Near Infrared (NIR) bands. For this task, the DJI Mavic 3M multispectral UAS system was employed. This system is equipped with a single Complementary Metal-Oxide-Semiconductor (CMOS) sensor for collecting high-resolution images in the visible spectrum, as well as 4 CMOS sensors that allow the acquisition of single-band images at specific wavelengths: Green (560 nm ± 16 nm), Red (650 nm ± 16 nm), RE (730 nm ± 16 nm), and NIR (860 nm ± 26 nm). Table 2 provides the specifications for the adopted equipment. In this regard, it should be underlined that the photogrammetric acquisitions using all five sensors were performed simultaneously to ensure that the sunlight conditions on the ground remained as consistent as possible. To this end, the downwelling light sensor (DLS) embedded in the UAV was employed. The DSL measures the solar irradiance for each of the five bands at the moment of image acquisition. This information, recorded in the image metadata, is used during the post-processing workflow, specifically in the reflectance calibration phase, to correct for lighting variations that occurred during the flight. The DLS was employed in place of a traditional reflectance calibration panel -despite the latter's potential for greater calibration accuracy (Ortega-Terol, Hernandez-Lopez, Ballesteros, & Gonzalez-Aguilera, 2017; da Silva, Gomes Pereira, Oliveira, 2024)– in order to propose a rapid and operationally efficient acquisition, aligned with the goals of this study as a rapid screening approach. Additionally, to enhance the ability of the reflected radiation response from wavelengths in the non-visible range of the electromagnetic spectrum to identify possible submerged structures (Änäkkälä, Lajunen, Hakojärvi, & Alakukku, 2022; de Souza et al., 2021), the flights were repeated both in the morning and afternoon, also complying with the constraints imposed by the archaeological park,. This allowed for a comparison between the effects of different sunlight conditions on the ground and while the two chosen times of flight helped in the mitigation of the hotspot effect (Ortega-Terol et al., 2017), common in multispectral imagery. In fact, the selected acquisition time proved to be the most suitable for minimising such effects in the captured imagery, considering the location and summer season (Pepe, Fregonese, Scaioni, 2018).

The flight planning was carried out considering several crucial aspects. The mission was designed with the sensor oriented at nadir and with both horizontal and vertical image overlaps of approximately 80%. These strategies were adopted to minimise angular distortions and also reduce reflectance-related effects, such as the bidirectional reflectance distribution function (BRDF), which, as the hotspot, is a common phenomenon in multispectral acquisition (Andrés-Anaya et al., 2024). It manifests as significant differences in brightness between images taken with the sun behind the sensor (backscatter), which appear noticeably brighter, and those taken with the sensor facing the sun. These variations affect reflectance accuracy and, consequently, the quality of derived products such as reflectance-based maps (Maes, 2025). Although models have recently been proposed to correct for this effect, they are not yet widely implemented in standard workflows for generating Analysis Ready Data (ARD) products, mainly due to their practical complexity (Andrés-Anaya et al., 2024). In this case study, they were not applied, in line with the overall objective of adopting a rapid and streamlined acquisition approach. Instead, efforts were focused on mitigating these effects during flight planning, as described above.

Due to the presence of trees, the flight altitude was planned to avoid interference with the foliage, while ensuring a GSD of approximately 1 cm, as regards the traditional visible images, and 2 cm, as regards the multispectral photogrammetric block. This was done to guarantee an appropriate resolution and the desired level of detail. The flight altitude that ensured a balance between these two parameters was approximately 50 m, based on the sensors of the DJI Mavic 3 UAV system's cameras.

During the flight planned according to the parameters outlined in the previous paragraphs, each sensor collected a total of 260 nadir images. Consequently, the photogrammetric block composed of traditional visible images consists of 260 images, while the multispectral block contains 1040 images (260 × 4 bands). The average acquisition distance —considering the previous factors related to authorised altitudes and site environmental constraints— ranged between approximately 49 and 52 m, resulting in a GSD of ca. 1.5 cm for the visible imagery and ca. 2.5 cm for the multispectral imagery. This difference is due to the considerably smaller sensors used for acquiring the multispectral dataset (Table 2).

Moreover, the multispectral dataset underwent reflectance calibration using the algorithm embedded in the processing software (Agisoft Metashape), which leveraged the data collected by the DLS to perform this correction. The use of the GCPs strategy for the absolute orientation, which optimises the photogrammetric bundle adjustment and the estimation of the image centre projection positions, along with Check Points (CPs) to assess the final metric accuracy of the computed point model, represents a significant bottleneck in the workflow of aerial remote sensing with UAVs. However, although the collimation of points in all four projects is certainly time-consuming, it greatly enhances the co-registration of the different blocks of multispectral single-band images, which otherwise could be slightly misaligned, particularly when using commercial sensors.

**Table 2**: Main specifications of DJI Mavic 3M visible camera and multispectral sensors.

| *UAS Model* | *DJI Mavic 3M* |
|---|---|
| *Optical sensor* | |
| Sensor type | 4/3'' CMOS |
| Sensor size | 17.3 × 13 mm |
| Effective pixel | 20 [MP] |
| Focal length | 12.29 mm; 24 mm |
| Lens field | 84° |
| Image size | 5280 × 3956 [pixel] |
| *(4) Multispectral sensors* | |
| Sensor type | 1/2.8'' CMOS |
| Sensor size | 5.2 mm × 3.9 mm |
| Effective pixel | 5 [MP] |
| Focal length | 4.34 mm; 25 mm (35 mm equivalent focal range) |
| Lens field | 73.91° |
| Image size | 2592 × 1944 [pixel] |
| Wavelength (Green – G) | 560 ± 16 nm |
| Wavelength (Red – R) | 650 ± 16 nm |
| Wavelength (Red Edge – RE) | 730 ± 16 nm |
| Wavelength (Near Infrared – NIR) | 860 ± 26 nm |

Tables 3 and 4 present the main technical results of the optical and multispectral image block orientations and point cloud computations. Table 4 provides the metric quality results, showing the average Root Mean Square Error (RMSE) of CPs as under 0.035 m (approximately twice the GSD value) for the visible projects. These values are consistent with the precision of the methods used and with the scale at which the survey was carried out, in line with the objectives of this research. The results of two multispectral dataset orientations are relatively higher. This is due, on one hand, to the fact that the GSD of the multispectral dataset is higher (with an approximate 2:1 ratio), and on the other hand, to the fact that, in this case, the photogrammetric process is characterised by greater complexity. However, considering that the goal of this research is to explore the potential presence of buried structures in the subsoil, the computed mean RSME values of ≤0.050 m and ≤0.080 m for the GCPs and CPs, respectively, can be considered acceptable.

Once the metric quality has been evaluated, all the added values photogrammetric products can be generated, always considering the DSM derived from the visible block as the best source for the height data. Overall, an orthophoto was generated for each photogrammetric block (Fig. 5). These orthophotos will serve as primary data for the analyses presented in the following sections.

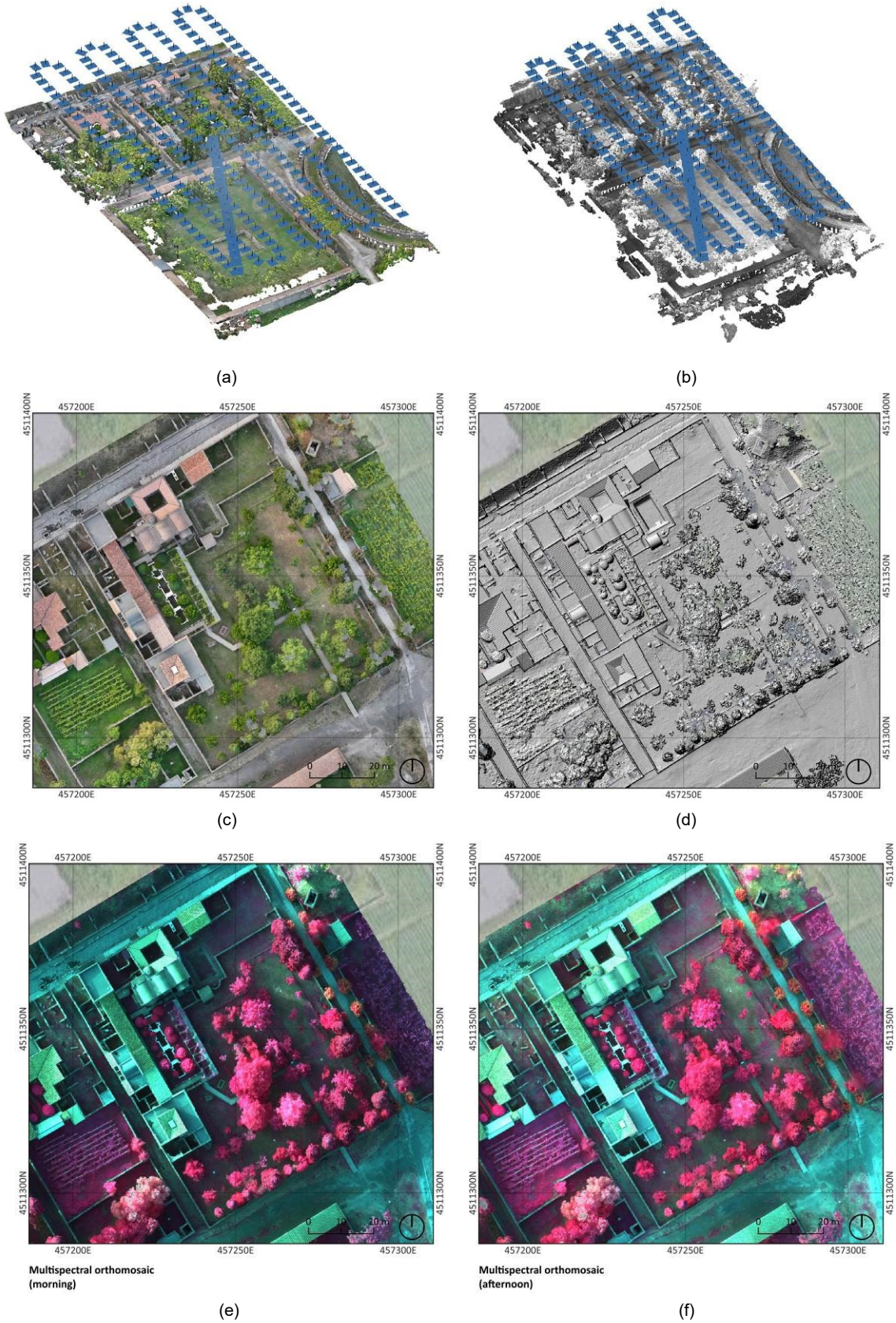


**Figure 5**: Main results derived from UAS photogrammetric process: (a) Dense cloud (visible dataset); (b) Dense cloud (multispectral dataset); (c) Orthophoto (visible dataset); (d) Shaded DSM (visible dataset); (e) Multispectral false-colour visualisation of orthophoto from morning dataset (NIR-RED-GREEN visualisation); (f) Multispectral false-colour visualisation orthophoto from afternoon dataset (NIR-RED-GREEN visualisation).

**Table 3**: The main results of the four image block orientations.

| | *N. images* | *Tie points* | *Dense cloud* | *Estimated GSD [cm/pixel]* |
|---|---|---|---|---|
| Optical dataset (Morning) | 260 | 504410 | 73615418 | 1.3 |
| Optical dataset (Afternoon) | 260 | 508131 | 77032851 | 1.3 |
| Multispectral dataset (Morning) | 260 × 4 bands | 1934385 | 38131831 | 2.3 |
| Multispectral dataset (Afternoon) | 260 × 4 bands | 2158407 | 39101160 | 2.3 |

**Table 4**: The main metric accuracy results for the processed photogrammetric blocks orientation in the visible and multispectral domains.

| | | *RMSE [m]* | | | |
|---|---|---|---|---|---|
| | | *X* | *Y* | *Z* | *XYZ* |
| Visible (Morning) | GCPs [12] | 0.008 | 0.013 | 0.015 | 0.017 |
| | CPs [9] | 0.015 | 0.013 | 0.020 | 0.035 |
| Visible (Afternoon) | GCPs [12] | 0.007 | 0.008 | 0.009 | 0.014 |
| | CPs [9] | 0.003 | 0.006 | 0.026 | 0.027 |
| Multispectral (Morning) | GCPs [12] | 0.041 | 0.028 | 0.007 | 0.050 |
| | CPs [9] | 0.054 | 0.045 | 0.037 | 0.080 |
| Multispectral (Afternoon) | GCPs [12] | 0.040 | 0.028 | 0.008 | 0.049 |
| | CPs [9] | 0.060 | 0.0.34 | 0.026 | 0.074 |

## 2.3. Multispectral data analysis

The two generated multispectral orthophotos were analysed using the same approach, namely by calculating spectral index maps. This is a well-established approach in visual photointerpretation, used to enhance and facilitate the investigation of the different spectral responses of surveyed elements, thereby aiding the detection of anomalies (Jackson & Huete, 1991; Nilsson, 1995). Among the adopted indices are those commonly used and consolidated in the literature for anomaly detection in archaeological contexts, particularly in satellite-based applications, which, however —due to the specific bands involved— can also be applied to UAV-based multispectral imagery (Ronchi et al., 2020). Building on this foundation —and taking into account relevant references, previous UAV-based applications, and the specific environmental conditions of the study area— the analysis focused on a subset of indices.

Specifically, Vegetation Indices (VIs) and Soil Indices (SIs) were considered to assess how the conditions of both the vegetation and soil in the *praedia hortus* and garden, as well as their response to buried artefacts and structures.

Among the VIs, the Normalized Difference Vegetation Index (NDVI) is one of the most commonly used spectral indices in remote sensing applications (Zhao & Qu, 2024), ranging from precision agriculture (Fabbri, Delgado, Guerrini, & Napoli, 2025) to archaeological investigations (Agapiou & Hadjimitsis, 2011; Uribe et al., 2015). It expresses the normalised ratio between the reflected energy in the red (RED) band, which is absorbed by the chlorophyll, and the reflected energy in the NIR, which is due to the scattering of light by theleaves. This provides an indicator of the health and greenness of the vegetation (Delegido et al., 2013). NDVI values range from -1 to +1: negative values indicate water bodies, values close to zero correspond to surfaces like rocks, sand, or concrete, while positive values are associated with various types of vegetation, including crops, shrubs, grasses, and forests. These values tend to approach +1 as the vegetation becomes healthier, denser, and in good condition (Huang, Tang, Hupy, Wang, & Shao, 2021). The NDVI index (Fig. 6) can be calculated using the following formula:

$$NDVI = \frac{(NIR - RED)}{(NIR + RED)} \quad (1)$$

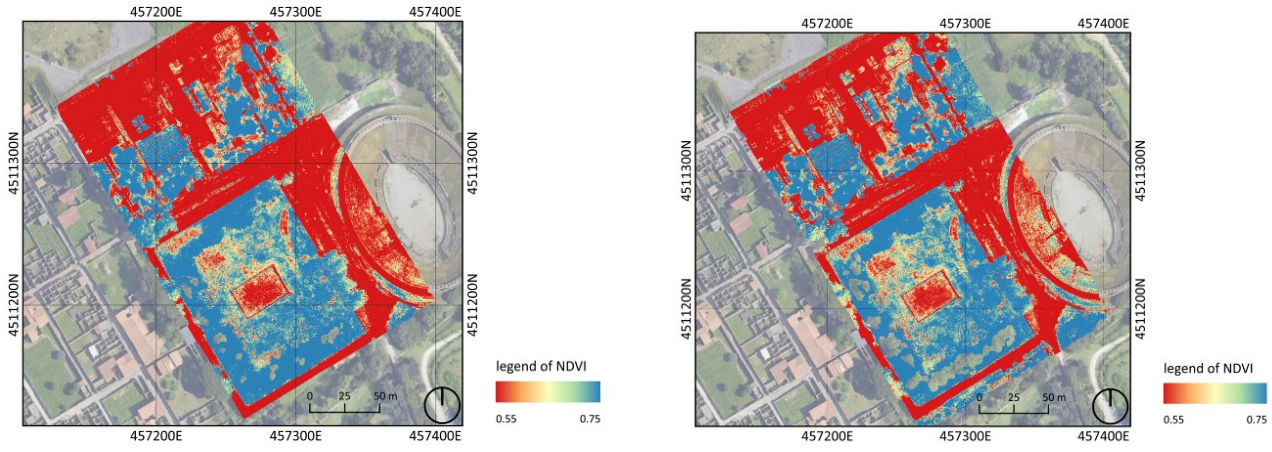


(a) (b)

**Figure 6**: NDVI index maps calculated from multispectral orthophotos derived by: (a) the morning flight dataset; and (b) the afternoon flight dataset.

The Enhanced Vegetation Index —2 (EVI 2) is derived from the Enhanced Vegetation Index (EVI), but it excludes the Blue (BLUE) band in the calculation. The BLUE band is typically used for noise reduction and to account for atmospheric aerosol variations. However, omitting it allows the index to be calculated even when the acquiring sensors, such as the one used in Pompeii, do not capture the BLUE band. EVI 2 considers environmental factors such as atmospheric conditions and soil background, offering improved vegetation monitoring (Abate & Lasaponara, 2019; Jiang, Huete, Didan, & Miura, 2008; Matsushita, Yang, Chen, Onda, & Qiu, 2007). Similar to the NDVI, EVI-2 yields positive values for vegetated areas and values close to zero or negative for rocky or water surfaces. Notably, the positive values of EVI-2 allow for a more precise discrimination of vegetation greenness, increasing sensitivity to variations among high values approaching +1, which are often challenging to interpret using NDVI (Jiang et al., 2008). The EVI 2 index (Fig. 7) can be calculated using the following formula:

$$EVI\ 2 = 2.5 \times \frac{(NIR - RED)}{NIR + (2.4 \times RED) + 1} \quad (2)$$

Lastly, the Normalized Difference Red Edge (NDRE) differs from the other indices as it also considers the contribution of the RE band (Ronchi et al., 2020). It is related to the chlorophyll content in vegetation and is particularly useful for monitoring crop health. NDRE values typically range between -1 and +1. Values from -1 to 0.2 generally correspond to bare soil or early-stage crops, while values between 0.2 and 0.6 are indicative of vegetation that is either stressed, unhealthy, or in an early growth phase. Values above 0.6 up to 1 are usually associated with healthy, mature, and ripening crops (Marx et al., 2024). The NDRE index (Figure 8) can be calculated using the following formula:

$$NDRE = \frac{(NIR - RE)}{(NIR + RE)} \quad (3)$$

Since the surveyed area also includes bare soil and sparsely vegetated ground, the use of SIs was also considered valuable. Specifically, the Brightness Index (BI) (Huang et al., 2024) was calculated to account for soil characteristics, which, in Mediterranean-type landscapes with irregular rainfall, such as the one in Pompeii, yield good results in identifying archaeological structures (Agapiou, Alexakis, Sarris, & Hadjimitsis, 2013; Salgado Carmona et al., 2020). The calculated

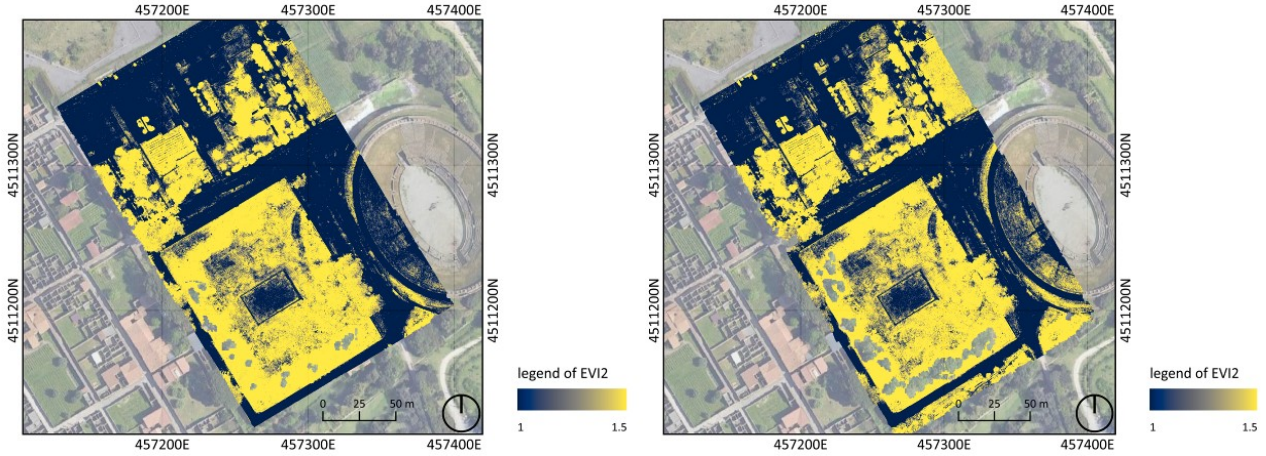


(a) (b)

**Figure 7**: EVI 2 index maps calculated from multispectral orthophotos derived by: (a) the morning flight dataset; and (b) the afternoon flight dataset.

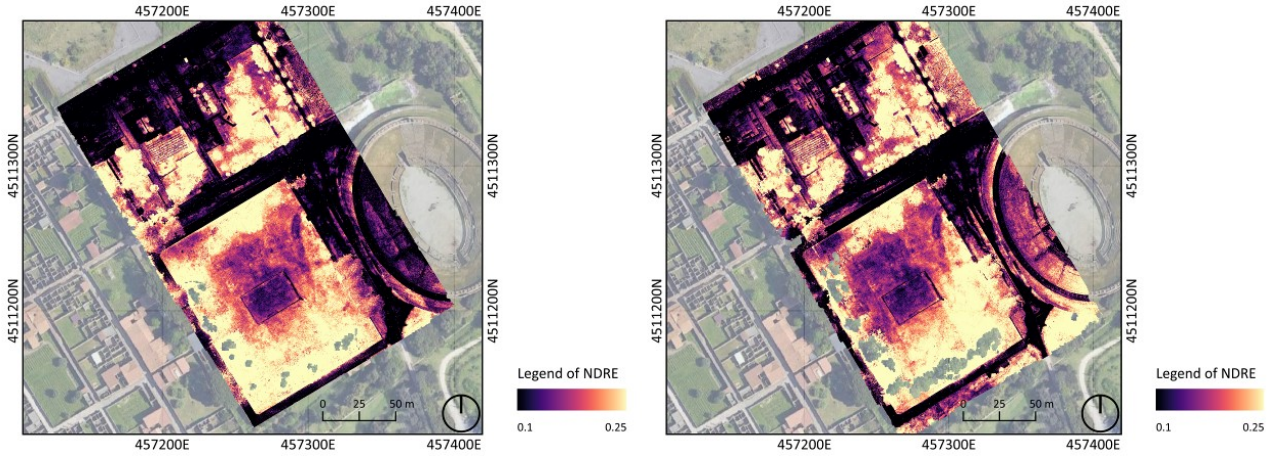


(a) (b)

**Figure 8**: NDRE index maps calculated from multispectral orthophotos derived by: (a) the morning flight dataset; and (b) the afternoon flight dataset.

index reflects the conditions of the soil surface, specifically indicating lower values for non-vegetated mineral surfaces, followed by bare soil, then soil with sparse vegetation, and higher values for areas covered by dense vegetation (Abderrazak, Kadhem, El Battay, Mohamed, & Rouai, 2016; Marques, Alvarez, Carral, Sastre, & Bienes, 2020). The BI index (Fig. 9) can be calculated using the following formula:

$$BI = \sqrt{\frac{(RED^2 + GREEN^2)}{2}} \quad (4)$$

Additionally, in this study, another index was tested. In other archaeological contexts, this index has shown particularly promising results in detecting non-visible features associated with underground structures. The RN index (RED + NIR) was successfully applied in a previous archaeological study using satellite imagery. It is a simple combination of the R and NIR bands, leveraging the spectral characteristics of vegetation in these wavelengths (Zanni & De Rosa, 2019). The RN index (Fig. 10) can be calculated using the following formula:

$$RN = RED + NIR \quad (5)$$

The calculation of the spectral indices —whose results are false colour maps (Figs. 6-10)— was performed using the multispectral and multiband orthophotos. The subsequent visual interpretative analysis was carried out in a Geographic Information System (GIS) environment, exploiting the possibility of using advanced tools for band management and their representation. For this task, the well-known open-source software QGIS was used. The use of this software enabled the possibility of managing heterogeneous data in a single environment, with the ability to efficiently relate them. In this case, considering the UAS-acquired data, the possibility to overlay and compare the multispectral data with the optical orthophoto and the DTM was crucial for the analysis. It also played a key role in preventing misinterpretation of spectral indices caused by canopy shadows or other elements within the surveyed areas. Moreover, georeferencing different datasets within the same environment –as will be discussed in the following sections– enabled cross-correlation between the results of the spectral index maps and the geophysical and archaeological investigations. This, in turn, provided deeper insights into the site and allowed a comparison between the multispectral analysis with the already known data.

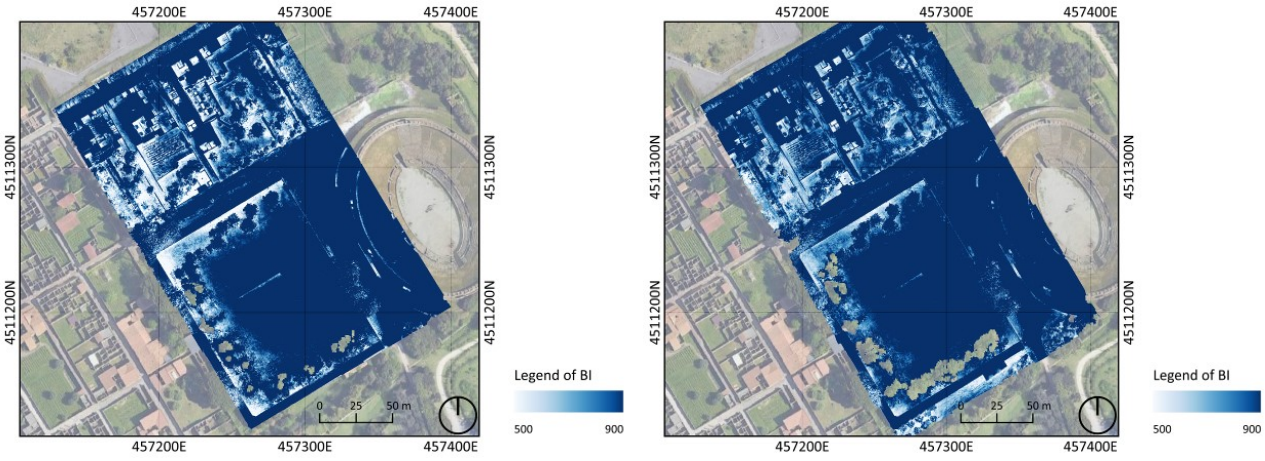


(a) (b)

**Figure 9**: BI index maps calculated from multispectral orthophotos derived by: (a) the morning flight dataset; and (b) the afternoon flight dataset.

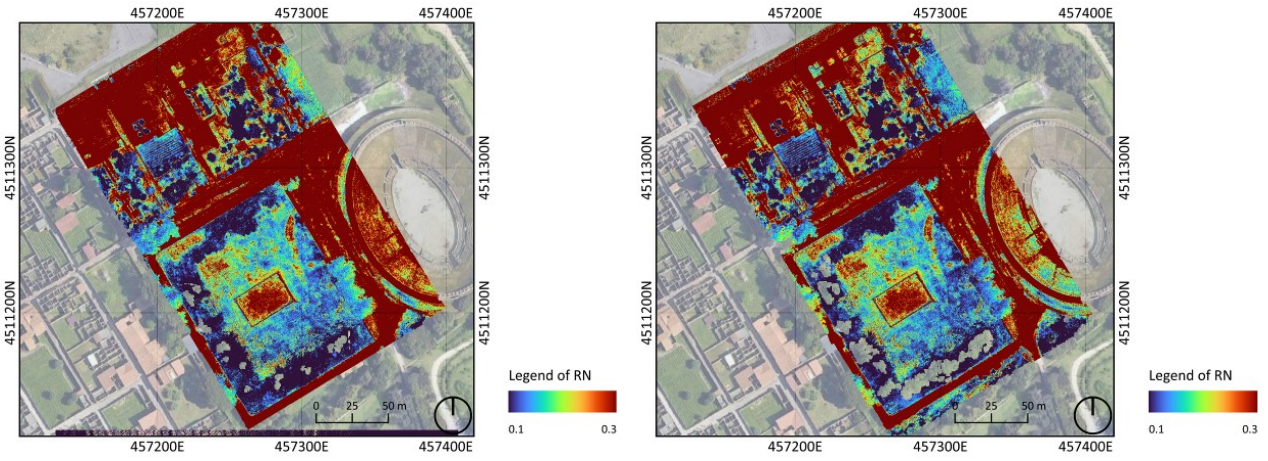


(a) (b)

**Figure 10**: RN index maps calculated from multispectral orthophotos derived by: (a) the morning flight dataset; and (b) the afternoon flight dataset.

## 3. Results

Since previous archaeological excavations and geophysical investigations have indicated the presence of walls associated with a water drainage system or channels for water distribution —likely connected to hydric conservation basins and fountains— it was considered beneficial to generate a DTM of the *Preaedia* complex. This DTM —derived from the DSM after the digital removal of trees by means of manual segmentation of the point cloud— clearly indicates a very regular slope in *hortus* area, approximately following a north-south direction. The contour lines, extracted at 10 cm intervals, unambiguously reflect the current organisation of the individual land plots, divided by the walkways of the visitor path and by hedges. However, this does not affect the overall slope trend, which decreases in the direction of the amphitheatre, presenting a height difference of more than 1.5 m between the two sides of the *insula* (Fig. 11). These elements could be further helpful for the future interpretation of spectral anomaly directions enlightened by index maps. The results of the comparative visual interpretation of each pair of index maps (derived from the morning and afternoon acquisitions), along with the subsequent integrated analysis enabled by their superposition, allow for the identification of several spectral anomalies. These anomalies are presented in the next section (Fig. 12).

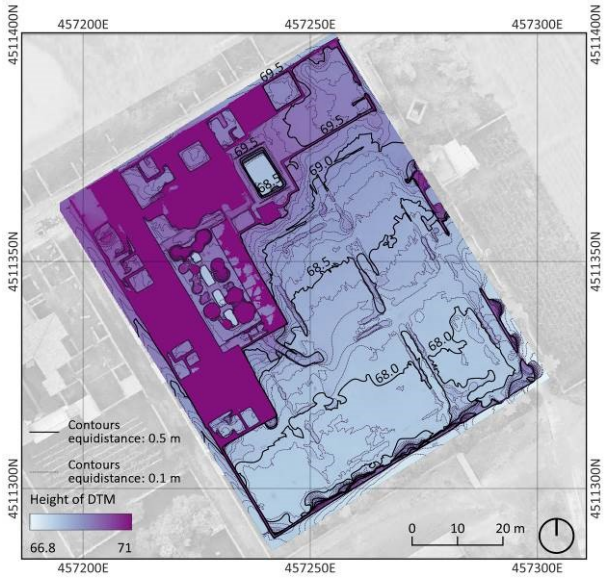


**Figure 11**: DTM representation derived from DSM (visible dataset) after trees removal. The DTM was interpolated only in the areas without the building, while its roof was not removed, and represented from the original DSM.

### 3.1. Spectral anomalies detection from index maps visual inspection

The detected spectral anomalies require considerable attention, as they may be caused by ancient, buried structures —whose presence in the *hortus* of the *Praedia* is confirmed— but could also result from modern drainage or irrigation systems.

The maps shown in Fig. 12 are organised in a three-column layout. The first column displays the index maps, while the second column presents the geometric vectorisation of the spectral anomalies, enlightened in different colours and overlaid on a low-opacity visible orthophoto. Finally, the third column presents the previously identified anomalies overlaid on the full-opacity visible orthophoto, in order to provide better contextualisation for the detected anomalies. Each row in the figure presents the results associated with a specific type of spectral index map: NDVI in the first row, EVI 2 in the second, NDRE in the third, BI in the fourth, and RN in the fifth. The first column displays the index maps extracted from the afternoon datasets, which exhibit a richer presence of spectral anomalies when compared to the corresponding index maps derived from the morning flight.

- The NDVI index map highlights linear anomalies located at the northern edge of the *insula* near the buildings used for commercial purposes (also within the thermal area); a series of anomalies located in the *viridarium*, the garden with a fountain made up of geometrically shaped mixtilinear basins at the centre of the *insula*, which could correspond to modern water supply infrastructures; a series of anomalies located in the area immediately south of the *viridarium* and the southern entrance to the *praedia*, aligned in a northeast-southwest direction; an anomaly along the perimeter wall that divides the *hortus* from the alley of the *preaedia* that surrounds the *insula* on the southwest side; some anomalies in the southern portion aligned with the line of maximum slope of the land.
- The EVI 2 index map presents a situation similar to the NDVI map, with some significant differences in the central part of the *hortus*. In this area, the anomalies appear less numerous in the proximity of the entrance walkway to the *praedia* from the garden. These anomalies still indicate a northeast-southwest direction, but they are characterised by a more elongated mark that turns at right angles and are aligned with the main directions of the *praedia* walls.
- The NDRE index map presents a situation only partially similar to the previous ones, as the anomalies in the areas of the commercial shops and the thermal area decrease; a linear anomaly is confirmed along the edge of the terrace to the north, with an areal spectral anomaly observed at the base of the terrace's height difference, south to the *natatio* of the thermal buildings, where Parslow identified drainage systems after conducting some trench excavations (Anguissola & Olivito, 2022c; Parslow, 1988); in the central area of the entrance walkway to the *praedia*, the spectral anomalies previously identified are confirmed, though they appear less numerous.
- The BI index map confirms anomalies already detected, distributed in the areas previously investigated, with particular confirmation of the marks in the southern area of the *hortus*, aligned with the direction of the maximum slope of the land, and the boundary wall along the *praedia* alley.
- The RN index map presents a situation of detected anomalies very similar to those found by reading the EVI 2 index map.

| *Index Map* | *Anomalies detection* | *UAV Map* |
|---|---|---|
| 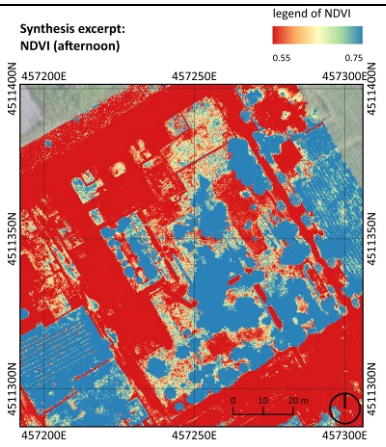 | 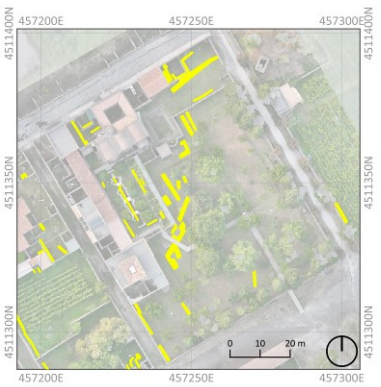 | 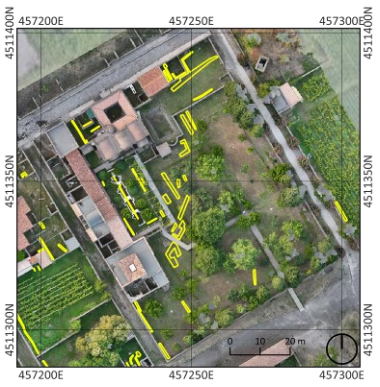 |
| 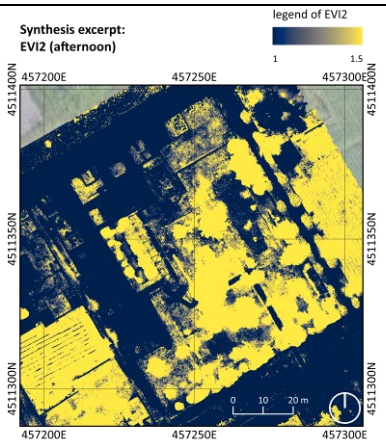 |  |  |
| 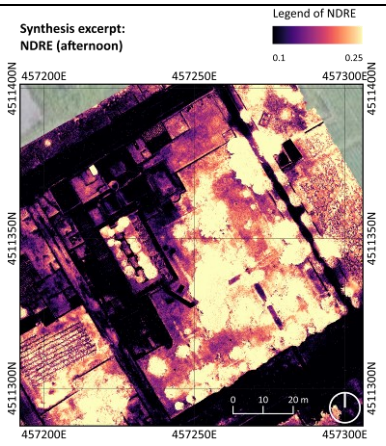 | 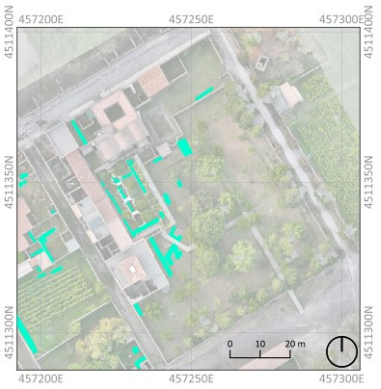 | 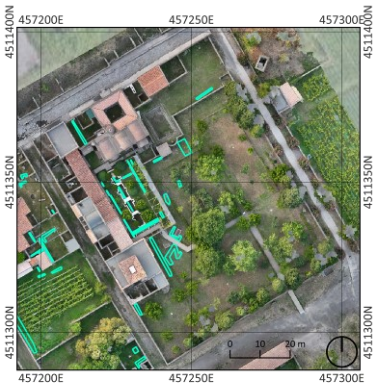 |
| 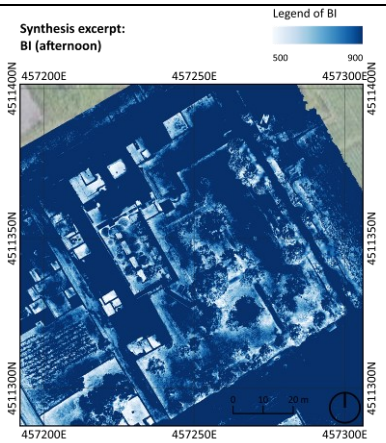 | 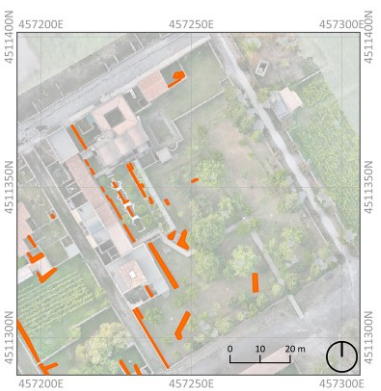 |  |

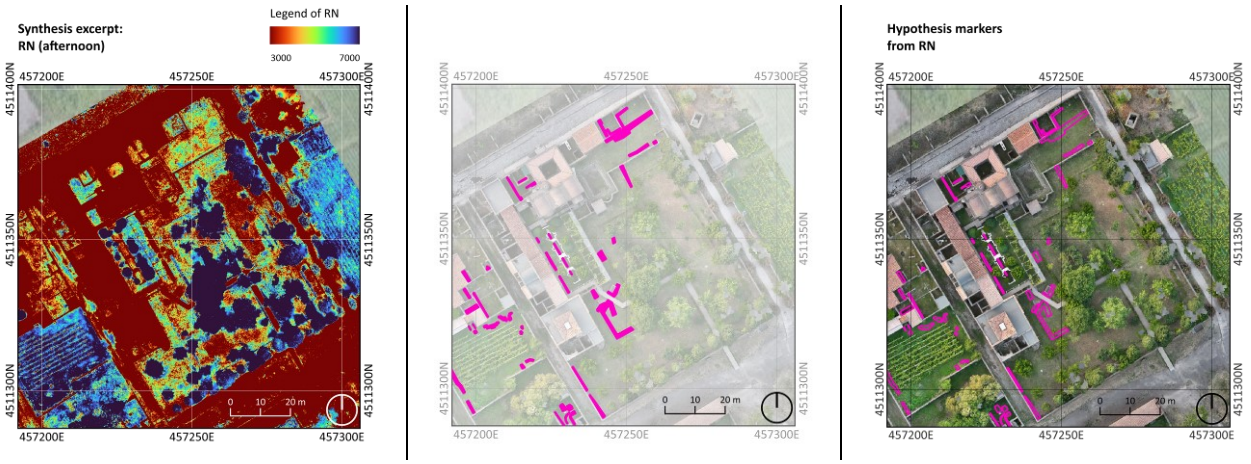


**Figure 12**: Schematic synthesis of comparison among single index maps (NDVI, EVI 2, NDRE, BI and RN), enhancing in different colours anomalies detected and shown overlapping the optical orthophoto.


**Figure 13**: Synthesis of the anomalies detected through the analysis of the five index maps, displayed overlaid on the RGB orthophoto. Each anomaly is represented in a different colour, corresponding to the specific index map in which it was identified, and is shown with partial transparency to facilitate visual overlap and comparison.

Lastly, a comprehensive map (Fig. 13) synthesises all crop marks identified through the applied indices, highlighted in different colours, each corresponding to the specific index represented in Figure 12.

A preliminary observation from the analysis of the different index maps is that using multiple index maps for anomaly detection has proven to be particularly effective. Since the indices are calculated in different ways and consider the contribution of various spectral bands, they exhibit different sensitivities depending on the different biomass, thickness and variety of vegetation in the considered areas.

For example, the EVI 2 index map was calculated to distinguish small differences between healthy and dense vegetation. As a consequence, it can be more effective in detecting anomalies where the standard NDVI index performs less effectively. In the case of the *praedia*, where the *hortus* exhibits a wide variety of vegetation types, with the aim of presenting to the public the possible ancient state of domestic crops and garden care (Anguissola & Olivito, 2022c; Spinosa, 2022), it is meaningful to consider these indices together, accounting for the different types of vegetation compared to the surrounding field land.

Furthermore, the different vegetation types and their specific phenological cycles provide a basis for testing these indices. The VI and SI, used in this study, were developed in the context of Earth RS land monitoring and classification, as well as in forestry and agriculture domains, primarily for small-scale datasets. While these indices have been widely used in literature for detecting archaeological remains in uniform crops and fields (Agapiou et al., 2013; Delegido et al., 2013; Moriarty et al., 2019), the continuous miniaturisation of sensors and the use of UAVs have enabled low-altitude, high-resolution acquisitions that capture fine-scale variations in vegetation. This higher spatial resolution allows spectral indices to be applied effectively even in more complex environments, including areas with heterogeneous, patchy or spontaneous vegetation, where plant species and canopy structures can vary considerably. In this context, the *praedia* vegetation provides an interesting, though not unique, case to test them (Peña-Villasenín, Gil-Docampo, & Ortiz-Sanz, 2024; Salgado Carmona et al., 2020).

As it has already been highlighted, however, not all anomalies presented in Fig. 13 can be confidently attributed to archaeological structures. In a complex stratified context such as Pompeii, some anomalies may correspond to features of different types, including modern interventions. Confirming the archaeological nature of these anomalies therefore requires an integrated approach, combining multispectral imagery with other investigative techniques, as proposed in the aims of this paper, which advocate an integrated and hierarchical strategy for site investigation.

## 4. Discussion

The analysis and identification of spectral anomalies in the index maps produced more extensive results than initially expected. Therefore, a detailed comparison was carried out with the information from the geophysical investigations (Marchetti et al., 2022; Urbini et al., 2021) (which, as mentioned in the previous sections, were

planned based on the stratigraphic excavations of the 1990s) and from the subsequent excavation tests carried out in 2019 and 2020, which were limited and specifically focused on directly examining the areas of interest suggested by the previous investigations. The initial steps involved collecting and selecting the most relevant geophysical survey maps, which provided key insights for the subsequent localisation of the stratigraphic samples carried out by the archaeologists. These maps were then compared with the results of the aerial remote sensing with UAV, using a common reference system within the GIS environment, which enabled a comparative analysis of both raster and vector data.

A further critical phase of the analysis aimed to synthesise the results of the spectral anomalies —derived from the analysis of the different index maps— in a single map. The frequency with which each index identified the same anomaly was quantified, and a confidence map was generated. This map summarises the findings using a gradient of red shades —ranging from more intense to less intense— based on the frequency of the anomaly occurrence across the different index maps (Fig. 14). Figure 14 presents in the first column three significant samples from the geophysical investigations: the first row shows a VMG map; the second row displays a 40 cm depth slice GPR map; the third row displays an 80 cm depth slice GPR map. The second column shows the most suitable index maps to perform the comparison, namely the NDRE index map and the RN index map. Finally, the map presented in the third column relates the data shown in the map of the first column with the essential information consisting of the projected shadow of the trees' canopy, together with the confidence mapping (on a normalised scale from 5 to 1) of the spectral index anomalies.

A first methodological consideration is the following: since index map can operate across areas with different types of vegetation (in terms of categories, densities, canopies' variety, etc.) and soil, the use of a large index range (such as -1 to 1) can be critical and increase the complexity of the visual interpretation. Anomaly detection may be more effective when focused on a narrower value range (e.g., 0.1 to 0.25), where subtle variations on the analysed surface are more likely to emerge (Fig. 15).

The stretching of the visualisation range enhances the contrast within the selected interval, thereby improving the readability and detectability of dominant patterns in the area of interest.

However, this process simultaneously attenuates variations at the extremes of the index scale —as illustrated in Fig. 14d— causing peripheral areas to appear saturated by a uniform colour. In contrast, within the focused range, tonal differences are more pronounced, allowing for a clearer distinction of values and more effective identification of anomalies. Therefore, it is important to underline that during the detection process, known results from archaeologists and geophysicists can offer valuable guidance in identifying the most appropriate index range for specific vegetation conditions in the targeted area. In this regard, it can be stated that the most critical issue posed by the presence of tree and shrub canopies is not limited to the areas directly covered, but also affects the surrounding zones, as canopy shapes and extents can vary over time.

This limitation was also considered when evaluating the spatial correspondence between the anomalies identified through multispectral analysis and those detected through other investigative methods (ground truth). For each comparison, a percentage-based assessment of the actual area of overlap was performed, considering also that UAV-based surveys are inherently restricted to areas not covered by dense vegetation.

Specifically in the comparison with geophysical techniques, it is important to highlight that this type of evaluation does not account for the different depths investigated by the two methods. While geophysical surveys —such as GPR— can detect features at various subsurface levels, multispectral imagery is limited to surface or near-surface signals. As a result, UAV-detected anomalies are more likely to correspond to shallow features and may not align with deeper anomalies revealed by geophysical methods. Therefore, cases where spatial overlap appears low —particularly when comparing UAV data with deeper GPR slices— do not necessarily reflect a failure in spectral anomaly detection, but rather the differing depth sensitivity of the two approaches. A more in-depth investigation into the comparison of such multi-source and heterogeneous datasets would certainly be worth pursuing in future research, with the aim of improving their integration and interpretative effectiveness.

Regarding the observations derived from the comparison of georeferenced data, the following key points can be highlighted:

- Pertaining to the first row of the image: geophysics specialists (Marchetti et al., 2022; Urbini et al., 2021) interpret the strong magnetic gradient values in the centre of the *hortus* as suggesting the presence of strongly magnetised elements at low depths. These elements probably have to be identified as modern buried hydric infrastructures. Instead, the anomaly along the northeast-southwest direction, which has weaker values, can be identified —in their opinion— with probable ancient structures. The index maps from aerial remote sensing with UAV also identified the same feature, as indicated by the circles on the two maps. This indicates a spatial overlap of around 62% between the anomalies detected through magnetic survey and those identified through spectral indices.
- Regarding the second and third rows of the image: both the GPR maps highlight different structures at the two considered depths (40 cm and 80 cm). The first anomaly (detected at 40 cm) corresponds to substructures of drainage systems, while the second map (depth 80 cm) shows a clear diagonal crossing masonry structure, which corresponds to the canal of the *Conte* of *Sarno* (Marchetti et al., 2022; Paone & Rispoli, 2011), which even the indices maps have easily identified despite the interruption due to the treetops. As expected, the correspondence between the anomalies detected through spectral indices and those derived from GPR is higher at shallower depths —approximately 62% at 40 cm— and decreases to around 45% when comparing with deeper slices, such as at 80 cm.

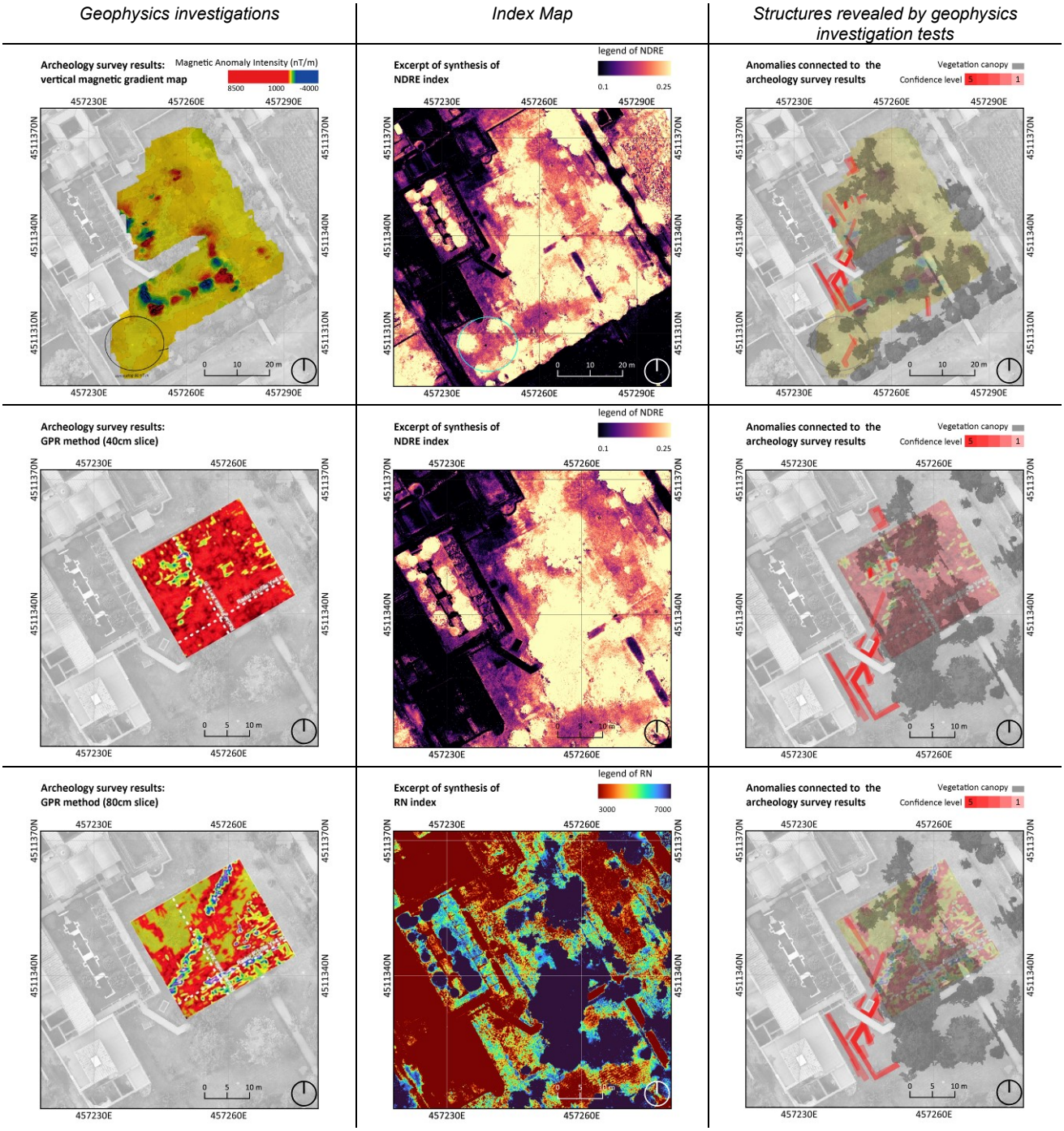


**Figure 14**: Synthesis of comparison among geophysical analysis maps (VMG and GPR, published in Marchetti et al. 2022 and reworked by the authors) with index maps (NDRE and RN indices), enhancing in red hues the confidence level of the spectral anomalies detected, confirmed by the other geophysical techniques.

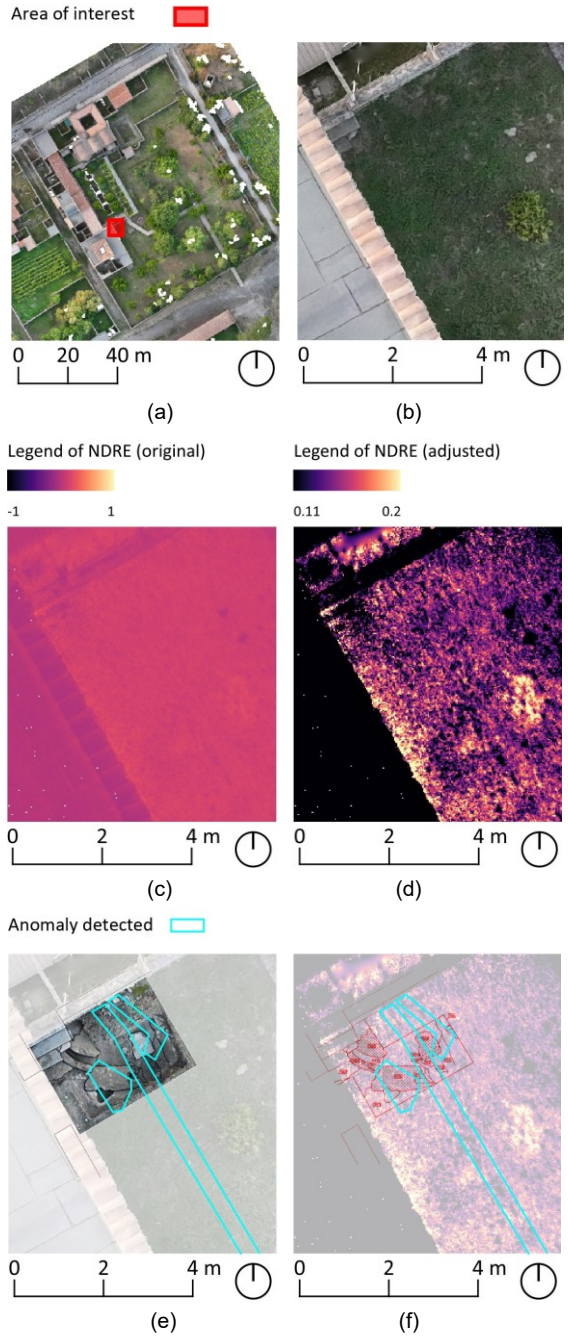


**Figure 15**: *Preaedia* of *Iulia Felix*: (a) RGB orthophoto; (b) RGB orthophoto detail; (c) NDRE map detail, displayed using the full standard range of the index values (-1 to 1); (d) (c) with the visualisation range stretched and limited to 0.11–0.2, allowing for a clearer representation and enhanced detection of the anomaly compared to the unstretched view; (e) Vectorisation of NDRE-derived anomalies overlaied on the trench orthophoto from the archaeological excavation (Anguissola & Olivito, 2022b), with the site orthophoto in the background; (f) Results of the archaeological excavation (red) and the vectorisation of the anomalies detected from NDRE index analysis (light blue), overlayed onto (d).

The archaeologists involved in the PRAEDIA project, following the geophysical investigations, carried out seven stratigraphic excavation trials in the *hortus* of *Iulia Felix praedia*. These excavations provided valuable information on channel systems and helped in the reconstruction of the urban landscape, prior to the construction of the *praedia* (Anguissola & Olivito, 2022b). Since the approach tested in the present research aimed to validate the capabilities of a relatively low-cost commercial sensor, used to develop aerial remote sensing with UAV survey presented in this manuscript, the focus was on the excavation areas that provided the most valuable insights from the archaeological work. As will be emphasised in the following paragraphs, the comparison between the results of the archaeological excavations and the anomalies identified herein highlights its effectiveness, also evidenced by the quantitative overlap assessment. In contrast to the geophysical data, which inherently involve a degree of uncertainty and complexity in interpretation, the results from the archaeological excavation allowed for a more straightforward and effective comparison.

The comparison between the archaeological results and those derived from the aerial remote sensing approach is presented in Figure 16, similarly to the one with the results of the geophysical surveys.

The first column shows the maps with the geolocalisation of the excavation tests perimeters from 2019-20. In the second column, the most significant index map is displayed. In the last column, the overlay of the confidence map is shown, summarising the spectral anomalies along with the projection of the treetops and a grayscale background orthophoto.

- First row: the archaeologists —prof. Anna Anguissola and prof. Riccardo Olivito— decided to open a series of excavation trenches near the *balneum* latrine (trenches 3, 4, and 6, highlighted in the map of the first row of the figure) to verify Parslow's hypothesis, which suggested the possible existence of a road that divided the *insula* into two parts (Anguissola & Olivito, 2022b). Although they did not find confirmation of the hypothesis regarding the road infrastructure, many walls with north-south and east-west orientation were identified, even in the index maps, despite the coverage of the treetops. In this case, the correspondence between the datasets is approximately 72 %, which is considered a good result, especially given the impact of tree cover on the analysed area.
- Second row: in areas 5 and 7, the archaeologists encountered the richest and most complex findings: while trench 5 revealed a small channel coming from the *viridarium*, area 7 uncovered a stratified set of different channels and a water cistern. They essentially identified three different channel systems originating from three different areas of the *praedia*, all directed towards the amphitheatre (Anguissola & Olivito, 2022b). In this case, the spectral anomalies of the index maps presented the most challenging situation, as marks are recognisable in all the different index maps. In this case, the excavation data confirmed the spectral anomalies with an accuracy of approximately 84 %. However, in both areas of interest, the overall context may have been partially affected by ground disturbances and backfilling activities that took place after the trench excavations were completed.

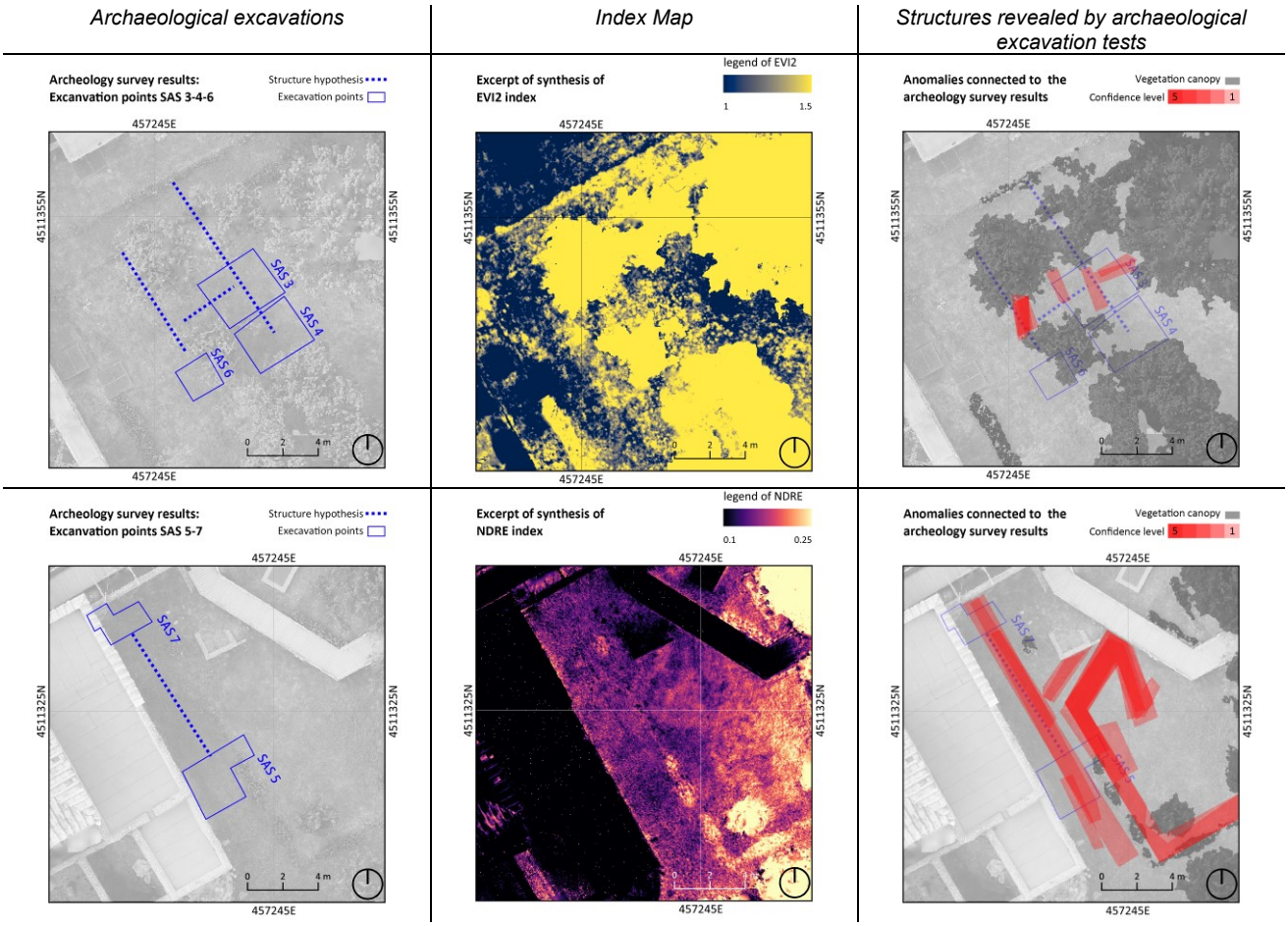


**Figure 16**: Synthesis of comparison among the geolocalisation of the archaeological trenches with index maps NDRE and EVI-2 indices, enhancing in red hues the confidence level of the spectral anomalies detected, confirmed by excavation activities.

Finally, a set of additional anomalies detected in areas not investigated by geophysical or archaeological surveys is presented. These anomalies are located in the small quadrant at the northernmost part of the *insula*, the *viridarium*, the area near the boundary wall with the *praedia* alley, and the region near the vineyard of the domus of the *Venere in Conchiglia*. Each of these areas is presented in the rows of Figure 17, with the first column displaying the index maps, the second column presenting the confidence maps of spectral anomalies, and the third column showing the visible orthophoto. The latter includes a higher-scale visualisation that clearly highlights the absence of visible marks in the visible range of the electromagnetic spectrum.

To conclude, based on the different aspects highlighted in the previous paragraphs, additional methodological considerations can be made:

- The detection process tends to be more straightforward in areas with limited human activity, compared to zones with significant anthropogenic disturbances.
- The numerous spectral anomalies and irregularities have been identified and deserve to be noticed. Most of them are located along buildings, structures, or streets, despite the absence of any visible signs in the UAV-derived optical orthophoto.
- The spatial relationships and connections between anomalies are particularly interesting and noteworthy, especially when the marks align in crossing or parallel formations, or coincide with one another, etc.
- In some cases, anomalies appeared as double lines in the index maps, potentially indicating the high precision and sensitivity of the method.
- The use of commercial UAV multispectral sensors certainly makes data acquisition much more efficient and cost-effective in terms of survey operations. However, when it comes to data analysis and the detection of anomalies, the limited availability of spectral bands —typically RE and NIR, in addition to two or three visible bands— can restrict the scope of detection. Specifically, the indices calculated in this research utilise two bands, RE and NIR, combined with visible bands in different ways. These bands, while contributing differently, are recognised as effective in detecting anomalies in vegetation and soil, as already presented in the previous paragraphs. In archaeological areas like Pompeii, where vegetation is rich and diverse, the acquisition and use of these bands —especially NIR— along with the combination of the RED band has proven effective for detecting anomalies related to buried archaeological structures.

RED and NIR, also considering the significant effort in modifying the original indices to be adapted to a reduced number of acquired bands (such as EVI and EVI 2) provide surely quite useful and valuable bands, effective in a cost-effective survey. However, it is certain that having access to additional bands, such as the BLUE in the visible spectrum or other sensors capable of acquiring TIR or SWIR data, could further enhance detection capabilities (Casana & Ferwerda, 2024).

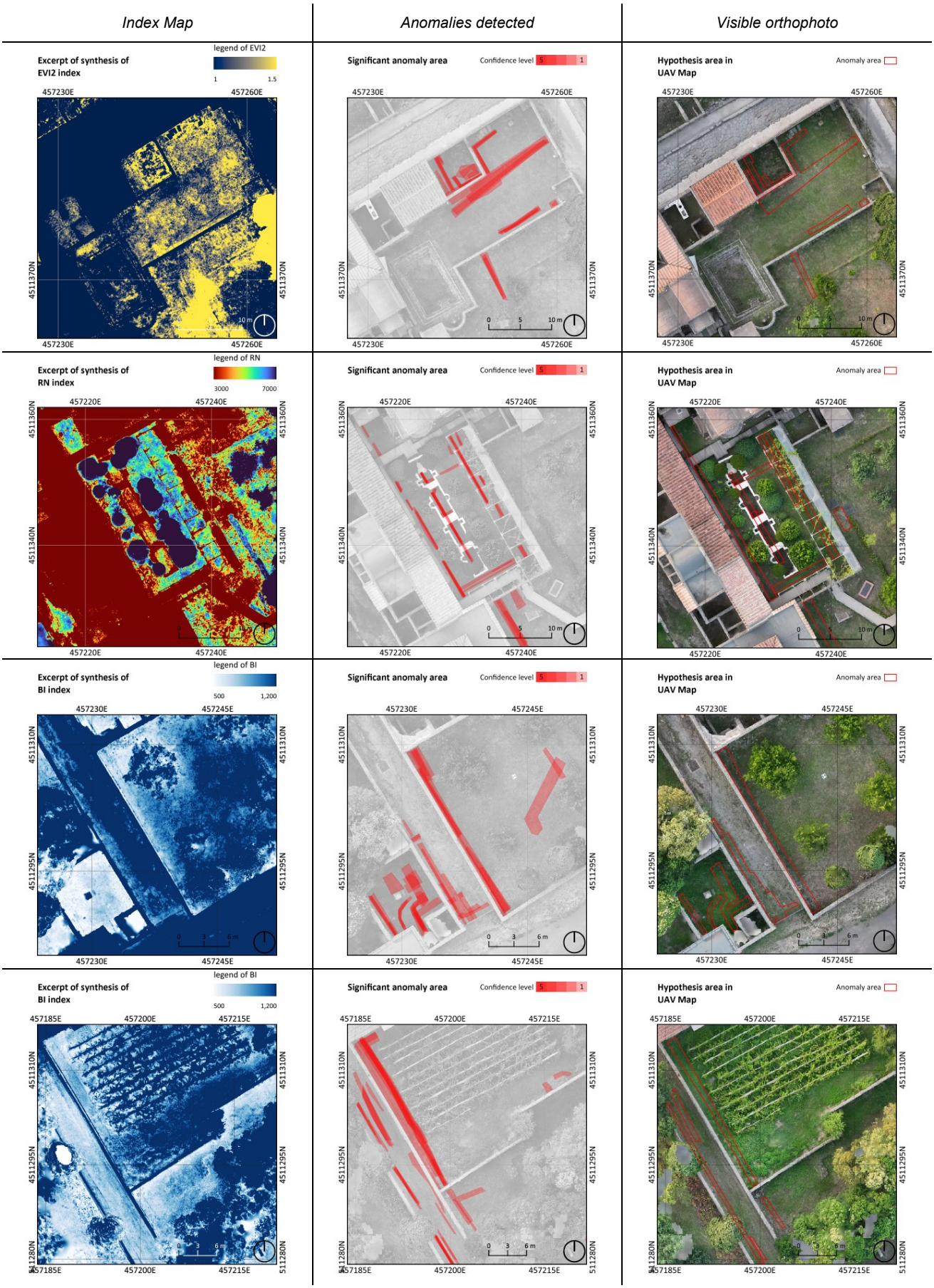


**Figure 17**: Summary of some significant anomalies (*Index map column*) in the northern part of the *insula*, within the alley of *praedia*, and in the vineyard of the domus of the *Venere in Conchiglia* displayed by the most effective index visualisation. The confidence map of the anomalies (*Anomalies detected column*) is then compared and overlaid with the RGB orthophoto (*Visible orthophoto column*), in which no visible signs potentially related to the anomalies can be identified.

## 5. Conclusions and future perspectives

The results achieved from the multispectral UAV photogrammetric survey at the *Praedia* of *Iulia Felix* demonstrate the promising potential of this methodology in detecting spectral anomalies that may correspond to buried archaeological features. The richness and consistency of the identified anomalies —many of which overlap with data from previous geophysical and archaeological investigations, with an average correspondence of approximately 65–70 %, despite the limitations encountered and the heterogeneity of the datasets— support the feasibility and effectiveness of using commercial multispectral UAV sensors for archaeological prospection.

These findings confirm the general workflow hypothesised at the beginning of the study: the use of multispectral imagery as a preliminary, extensive, and non-invasive knowledge tool for defining excavation areas' perimeters and, subsequently, refining targeted geophysical or archaeological investigations. At the same time, the carried-out analyses highlight the importance of prior knowledge of the surveyed site and its structures, particularly in the fine-tuning of spectral index map interpretations —for example, by narrowing the range of index values considered significant based on vegetation type and context. Surely, although the limited number of spectral bands acquired by commercial UAS sensors may constrain detection capabilities, the combined use of RED and NIR bands —especially considering existing indices specifically modified for reduced-band configurations— has proven to be particularly effective in complex environments like Pompeii. Both the considered aspects reinforce and enhance the value of integrating different survey techniques in a reciprocal and complementary manner, rather than employing them separately.

Furthermore, additional UAV-borne sensors may further support the detection process. For instance, UAV LiDAR represents an increasingly promising technology capable of providing high-resolution data even in densely vegetated areas where optical visibility is otherwise limited, thanks to the high penetrative capability of these sensors. These solutions enable the generation of high-resolution DTMs, useful for supporting research on archaeological sites or landscapes (Cappellazzo et al., 2024; Haryuatmanto, 2023).

As future perspectives, one aspect that deserves further investigation is the replicability of the method. The authors tested the suitability of the proposed method for the detection of submerged structures in Santoro et al. 2023, with the aim of identifying underground fortifications located in an Alpine context in northern Italy. In Fassbinder et al. 2025 (Fassbinder et al., 2025), despite the completely different context —in terms of vegetation in the area, as well as the material and construction type of the archaeological remains investigated —the use of UAV-based aerial remote sensing combined with GPR techniques was successfully tested in the ancient city of Seleucia on the Tigris (Iraq). These applications allow users to achieve accurate results despite the high heterogeneity of the investigated case studies. In a context such as that related to 3D metric documentation and archaeological monitoring, the development of\ procedures, standards, and best practices characterised by high repeatability is of significant importance. However, it is also crucial to ensure adequate flexibility that tailors these methods to archaeological sites with heterogeneous features, as in the case described in the current paper.

In this regard, Pompeii represents an ideal case study for this type of investigation, given the site's high heterogeneity —particularly regarding the stratigraphy and the types of soil and vegetation investigated. Currently, as mentioned in Section 2, further research focusing on the area corresponding to the *Palestra Grande* and surrounding regions is underway, involving a multidisciplinary collaboration between archaeologists and geophysicists, and is expected to be published soon.

From a methodological perspective, another aspect that should be underlined regards the manual visual interpretation of anomalies. This step, while essential, is particularly time-consuming due to the amount of spectral index maps involved, and also considering the site dimensions. This concerns both the data processing and the interpretation phases. With the aim of increasing the replicability of the method, while enhancing its sustainability, the development of semi-automated or fully automated anomaly detection procedures would be highly beneficial, especially when applied to larger datasets. Future research will therefore focus on investigating such approaches to improve both efficiency and repeatability. A perspective of significant interest concerns the use of artificial intelligence algorithms — specifically, using deep learning methods, which in recent years has emerged as the preferred and state-of-the-art method for tasks that involve image processing— to enhance the efficiency of these processes (Character et al., 2024; Yang et al., 2024).

## Acknowledgements

The experimental activities were developed within the framework of the PRAEDIA - Pompeian Residential Architecture: Environmental, Digital, Interdisciplinary Archive project, in agreement among the Archaeological Park of Pompeii, the University of Pisa, the IMT School of Advanced Studies of Lucca, the National Institute of Geophysics and Volcanology and Politecnico di Torino. For this reason, the authors would like to express their sincere gratitude to S. Bertesago, I. Cangiano (Archaeological Park of Pompeii), A. Anguissola (University of Pisa), and R. Olivito (IMT School of Advanced Studies of Lucca) for the invitation to cooperate on an extraordinary fieldwork at Pompeii. The initiative was primarily conceived as a training activity for students from the DIRECT Team of Politecnico di Torino, with dedicated funding for this purpose.

The doctoral position of Valentina Santoro is supported within the framework of the National Recovery and Resilience Plan —Next Generation EU (PNRR–NGEU) project, which has received funding from the Italian Ministry of Universities and Research (Ministero dell'Università e della Ricerca, MUR) under Decree No. 118/2023 (DM 118/2023).

## References

Abate, N., & Lasaponara, R. (2019). Preventive archaeology based on open remote sensing data and tools: the cases of Sant'Arsenio (SA) and Foggia (FG), Italy. *Sustainability*, *11*(15), 4145. https://doi.org/10.3390/su11154145

Abderrazak, B., Kadhem, G., El Battay, A., Mohamed, N., & Rouai, M. (2016). Assessment of land erosion and sediment accumulation caused by runoff after a flash-flooding storm using topographic profiles and spectral indices. *Advances in Remote Sensing*, *5*, 315–354. https://doi.org/10.4236/ars.2016.54024

Agapiou, A., Alexakis, D. D., Sarris, A., & Hadjimitsis, D. G. (2013). Orthogonal equations of multi-spectral satellite imagery for the identification of un-excavated archaeological sites. *Remote Sensing*, *5*(12), 6560–6586. https://doi.org/10.3390/rs5126560

Agapiou, A., & Hadjimitsis, D. G. (2011). Vegetation indices and field spectroradiometric measurements for validation of buried architectural remains: Verification under area surveyed with geophysical campaigns. *Journal of Applied Remote Sensing*, *5*(1), 053554. https://doi.org/10.1117/1.3645590

Agudo, P. U., Pajas, J. A., Pérez-Cabello, F., Redón, J. V., & Lebrón, B. E. (2018). The potential of drones and sensors to enhance detection of archaeological cropmarks: a comparative study between multi-spectral and thermal imagery. *Drones*, *2*(3), 29. https://doi.org/10.3390/drones2030029

Aicardi, I., Chiabrando, F., Grasso, N., LINGUA, A., Noardo, F., & Spano, A. (2016). UAV PHOTOGRAMMETRY WITH OBLIQUE IMAGES: FIRST ANALYSIS ON DATA ACQUISITION AND PROCESSING. *ISPRS - International Archives of the Photogrammetry, Remote Sensing and Spatial Information Sciences*, *XLI-B1*, 835–842. https://doi.org/10.5194/isprsarchives-XLI-B1-835-2016

Änäkkälä, M., Lajunen, A., Hakojärvi, M., & Alakukku, L. (2022). Evaluation of the Influence of Field Conditions on Aerial Multispectral Images and Vegetation Indices. *Remote Sensing*, *14*(19), 4792. https://doi.org/10.3390/rs14194792

Andrés-Anaya, P., Molada-Tebar, A., Hernández-López, D., Moreno, M. Á., González-Aguilera, D., & Herrero-Huerta, M. (2024). Radiometric improvement of spectral indices using multispectral lightweight sensors onboard UAVs. *Drones*, *8*(2), 36. https://doi.org/10.3390/drones8020036

Anguissola, A., & Olivito, R. (2022a). I Praedia di Iulia Felix alla luce delle nuove acquisizioni: Una sintesi. In *Edizione degli scavi nei Praedia di Iulia Felix e studi sulla Regio II di Pompei* (pp. 77–120). Pisa, Italy: Pisa University Press. https://www.academia.edu/95674889/A_Anguissola_R_Olivito_PRAEDIA_I_Edizione_degli_scavi_nei_Praedia_di_Iulia_Felix_e_studi_sulla_Regio_II_di_Pompei_Pisa_University_Press_Pisa_2022

Anguissola, A., & Olivito, R. (2022b). I saggi di scavo 2019-2020 nell'hortus dei Praedia di Iulia Felix. In *Edizione degli scavi nei Praedia di Iulia Felix e studi sulla Regio II di Pompei* (pp. 137–176). Pisa, Italy: Pisa University Press. https://www.academia.edu/95674889/A_Anguissola_R_Olivito_PRAEDIA_I_Edizione_degli_scavi_nei_Praedia_di_Iulia_Felix_e_studi_sulla_Regio_II_di_Pompei_Pisa_University_Press_Pisa_2022

Anguissola, A., & Olivito, R. (2022c). Introduzione. In *Edizione degli scavi nei Praedia di Iulia Felix e studi sulla Regio II di Pompei* (pp. 9–14). Pisa, Italy: Pisa University Press. https://www.academia.edu/95674889/A_Anguissola_R_Olivito_PRAEDIA_I_Edizione_degli_scavi_nei_Praedia_di_Iulia_Felix_e_studi_sulla_Regio_II_di_Pompei_Pisa_University_Press_Pisa_2022

Belcore, E., Pittarello, M., Lingua, A. M., & Lonati, M. (2021). Mapping Riparian Habitats of Natura 2000 Network (91E0*, 3240) at Individual Tree Level Using UAV Multi-Temporal and Multi-Spectral Data. *Remote Sensing*, *13*(9), 1756. https://doi.org/10.3390/rs13091756

Calleja, J. F., Requejo Pagés, O., Díaz-Álvarez, N., Peón, J., Gutiérrez, N., Martín-Hernández, E., … Fernández Álvarez, P. (2018). Detection of buried archaeological remains with the combined use of satellite multispectral data and UAV data. *International Journal of Applied Earth Observation and Geoinformation*, *73*, 555–573. https://doi.org/10.1016/j.jag.2018.07.023

Cappellazzo, M., Patrucco, G., Sammartano, G., Baldo, M., & Spanò, A. (2024). Semantic Mapping of Landscape Morphologies: Tuning ML/DL Classification Approaches for Airborne LiDAR Data. *Remote Sensing*, *16*(19), 3572. https://doi.org/10.3390/rs16193572

Casana, J., & Ferwerda, C. (2024). Drone-Acquired Short-Wave Infrared (SWIR) Imagery in Landscape Archaeology: An Experimental Approach. *Remote Sensing*, *16*(10), 1671. https://doi.org/10.3390/rs16101671

Cebrián, R., Hortelano, I., Ortiz, I., & Vallés, J. (2024). Detection of funerary monuments in the northern necropolis of Segobriga using multispectral and georadar imaging. *Virtual Archaeology Review*. https://doi.org/10.4995/var.2024.22738

Chao, H., Cao, Y., & Chen, Y. (2010). Autopilots for small unmanned aerial vehicles: A survey. *International Journal of Control, Automation and Systems*, *8*(1), 36–44. https://doi.org/10.1007/s12555-010-0105-z

Character, L., Beach, T., Inomata, T., Garrison, T. G., Luzzadder-Beach, S., Baldwin, J. D., … Ranchos, J. L. (2024). Broadscale deep learning model for archaeological feature detection across the Maya area. *Journal of Archaeological Science*, *169*, 106022. https://doi.org/10.1016/j.jas.2024.106022

Cigna, F., & Tapete, D. (2021). Satellite Technologies for Monitoring Archaeological Sites at Risk. In A. Traviglia, L. Milano, C. Tonghini, & R. Giovanelli, *Stolen Heritage  Multidisciplinary Perspectives on Illicit Trafficking of Cultural Heritage in the EU and the MENA Region* (p. Chapter_5510). Venice: Fondazione Università Ca' Foscari. https://doi.org/10.30687/978-88-6969-517-9/007

Costa, H., Benevides, P., Marcelino, F., & Caetano, M. (2020). Introducing automatic satellite image processing into land cover mapping by photo-interpretation of airborne data. *The International Archives of the Photogrammetry, Remote Sensing and Spatial Information Sciences*, *XLII-3-W11*, 29–34. https://doi.org/10.5194/isprs-archives-XLII-3-W11-29-2020

Council of Europe. (2005). *The Faro Convention*. Retrieved from https://rm.coe.int/1680083746

da Silva, T. v. d. W., Gomes Pereira, L., & Oliveira, B. R. F. (2024). Assessing Geometric and Radiometric Accuracy of DJI P4 MS Imagery Processed with Agisoft Metashape for Shrubland Mapping. *Remote Sensing*, *16*(24), 4633. https://doi.org/10.3390/rs16244633

Davis, D. (2021). Theoretical repositioning of automated remote sensing archaeology: shifting from features to ephemeral landscapes. *Journal of Computer Applications in Archaeology*, *4*(1). https://doi.org/10.5334/jcaa.72

de Souza, R., Buchhart, C., Heil, K., Plass, J., Padilla, F. M., & Schmidhalter, U. (2021). Effect of time of day and sky conditions on different vegetation indices calculated from active and passive sensors and images taken from UAV. *Remote Sensing*, *13*(9), 1691. https://doi.org/10.3390/rs13091691

Delegido, J., Verrelst, J., Meza, C. M., Rivera, J. P., Alonso, L., & Moreno, J. (2013). A red-edge spectral index for remote sensing estimation of green LAI over agroecosystems. *European Journal of Agronomy*, *46*, 42–52. https://doi.org/10.1016/j.eja.2012.12.001

Fabbri, C., Delgado, A., Guerrini, L., & Napoli, M. (2025). Precision nitrogen fertilization strategies for durum wheat: A sustainability evaluation of NNI and NDVI map-based approaches. *European Journal of Agronomy*, *164*, 127502. https://doi.org/10.1016/j.eja.2024.127502

Fassbinder, J., Lippolis, C., Messina, V., Patrucco, G., Santoro, V., & Spano, A. (2025). *Preliminary report on the campaigns 2022-2023 of the Italian Archaeological Expedition at Seleucia on the Tigris (IAES). Mesopotamia: rivista di archeologia, epigrafia e storia orientale antica: LIX, 2024*, 55-82. https://iris.polito.it/handle/11583/2997480

Fiz, J. I., Martín, P. M., Cuesta, R., Subías, E., Codina, D., & Cartes, A. (2022). Examples and results of aerial photogrammetry in archeology with UAV: Geometric documentation, high resolution multispectral analysis, models and 3D printing. *Drones*, *6*(3), 59. https://doi.org/10.3390/drones6030059

Gojda, M., & Hejcman, M. (2012). Cropmarks in main field crops enable the identification of a wide spectrum of buried features on archaeological sites in Central Europe. *Journal of Archaeological Science*, *39*(6), 1655–1664. https://doi.org/10.1016/j.jas.2012.01.023

Gupta, S. G., Ghonge, D. M., & Jawandhiya, P. M. (2013). Review of unmanned aircraft system (UAS). *International Journal of Advanced Research in Computer Engineering & Technology*, *2*(4). https://doi.org/10.2139/ssrn.3451039

Haryuatmanto, G. (2023). Analysis of airborne LiDAR data for archaeology study case: Sriwijaya Muaro Jambi Site. *IOP Conference Series: Earth and Environmental Science*, *1127*(1), 012012. https://doi.org/10.1088/1755-1315/1127/1/012012

Hill, A. C., Laugier, E. J., & Casana, J. (2020). Archaeological remote sensing using multi-temporal, drone-acquired thermal and near infrared (NIR) imagery: A case study at the Enfield Shaker Village, New Hampshire. *Remote Sensing*, *12*(4), 690. https://doi.org/10.3390/rs12040690

Hollesen, J., Jepsen, M. S., & Harmsen, H. (2023). The application of RGB, multispectral, and thermal imagery to document and monitor archaeological sites in the Arctic: a case study from South Greenland. *Drones*, *7*(2), 115. https://doi.org/10.3390/drones7020115

Huang, S., Tang, L., Hupy, J. P., Wang, Y., & Shao, G. (2021). A commentary review on the use of normalized difference vegetation index (NDVI) in the era of popular remote sensing. *Journal of Forestry Research*, *32*(1), 1–6. https://doi.org/10.1007/s11676-020-01155-1

Huang, T., Olsoy, P. J., Glenn, N. F., Cattau, M. E., Roser, A. V., Boehm, A., & Clark, P. E. (2024). Quantifying rangeland fractional cover in the Northern Great Basin sagebrush steppe communities using high-resolution unoccupied aerial systems (UAS) imagery. *Landscape Ecology*, *39*(11), 196. https://doi.org/10.1007/s10980-024-01983-0

Jackson, R. D., & Huete, A. R. (1991). Interpreting vegetation indices. *Preventive Veterinary Medicine*, *11*(3), 185–200. https://doi.org/10.1016/S0167-5877(05)80004-2

Jiang, Z., Huete, A. R., Didan, K., & Miura, T. (2008). Development of a two-band enhanced vegetation index without a blue band. *Remote Sensing of Environment*, *112*(10), 3833–3845. https://doi.org/10.1016/j.rse.2008.06.006

Johnson, K., Nissen, E., Saripalli, S., Arrowsmith, J. R., McGarey, P., Scharer, K., … Blisniuk, K. (2014). Rapid mapping of ultrafine fault zone topography with structure from motion. *Geosphere*, *10*(5), 969–986. https://doi.org/10.1130/GES01017.1

Kapari, M., Sibanda, M., Magidi, J., Mabhaudhi, T., Mpandeli, S., & Nhamo, L. (2025). Assessment of the maize crop water stress index (CWSI) using drone-acquired data across different phenological stages. *Drones*, *9*(3), 192. https://doi.org/10.3390/drones9030192

Lanaras, C., Bioucas-Dias, J., Galliani, S., Baltsavias, E., & Schindler, K. (2018). Super-resolution of Sentinel-2 images: Learning a globally applicable deep neural network. *ISPRS Journal of Photogrammetry and Remote Sensing*, *146*, 305–319. https://doi.org/10.1016/j.isprsjprs.2018.09.018

Luo, L., Wang, X., Guo, H., Lasaponara, R., Zong, X., Masini, N., … Yao, Y. (2019). Airborne and spaceborne remote sensing for archaeological and cultural heritage applications: A review of the century (1907–2017). *Remote Sensing of Environment*, *232*, 111280. https://doi.org/10.1016/j.rse.2019.111280

Machala, M., Honzova, M., & Klimánek, M. (2015). *Generating land-cover maps from remotely sensed data: Manual vectorization versus object-oriented automation*. Monash University. Journal contribution, *11*, 1–30. https://doi.org/10.4225/03/57D7990BEA4AC

Maes, W. H. (2025). Practical guidelines for performing UAV mapping flights with snapshot sensors. *Remote Sensing*, *17*(4), 606. https://doi.org/10.3390/rs17040606

Marchetti, M., Materni, V., Sapia, V., & Urbini, S. (2022). Indagini geofisiche nell'hortus dei Praedia di Iulia Felix. In *Edizione degli scavi nei Praedia di Iulia Felix e studi sulla Regio II di Pompei* (pp. 9–14). Pisa, Italy: Pisa University Press. Retrieved from https://www.academia.edu/95674889/A_Anguissola_R_Olivito_PRAEDIA_I_Edizione_degli_scavi_nei_Praedia_di_Iulia_Felix_e_studi_sulla_Regio_II_di_Pompei_Pisa_University_Press_Pisa_2022

Marques, M. J., Alvarez, A., Carral, P., Sastre, B., & Bienes, R. (2020). The use of remote sensing to detect the consequences of erosion in gypsiferous soils. *International Soil and Water Conservation Research*, *8*(4), 383–392. https://doi.org/10.1016/j.iswcr.2020.10.001

Marx, A., Clasen, A., May, J., König, S., Kleinschmit, B., & Förster, M. (2024). Imaging spectroscopy for bark beetle detection in Norway spruce and the relevance of the red-edge spectral range. *International Journal of Applied Earth Observation and Geoinformation*, *133*, 104100. https://doi.org/10.1016/j.jag.2024.104100

Masini, N., & Lasaponara, R. (2006). Satellite-based recognition of landscape archaeological features related to ancient human transformation. *Journal of Geophysics and Engineering*, *3*(3), 230–235. https://doi.org/10.1088/1742-2132/3/3/004

Masini, N., Romano, G., Sieczkowska, D., Capozzoli, L., Spizzichino, D., Gabellone, F., Lasaponara, R. (2023). Non invasive subsurface imaging to investigate the site evolution of Machu Picchu. *Scientific Reports*, *13*(1), 16035. https://doi.org/10.1038/s41598-023-43361-x

Matsushita, B., Yang, W., Chen, J., Onda, Y., & Qiu, G. (2007). Sensitivity of the enhanced vegetation index (EVI) and normalized difference vegetation index (NDVI) to topographic effects: a case study in high-density Cypress Forest. *Sensors*, *7*(11), 2636–2651. https://doi.org/10.3390/s7112636

Moriarty, C., Cowley, D. C., Wade, T., & Nichol, C. J. (2019). Deploying multispectral remote sensing for multi-temporal analysis of archaeological crop stress at Ravenshall, Fife, Scotland. *Archaeological Prospection*, *26*(1), 33–46. https://doi.org/10.1002/arp.1721

Nikolakopoulos, K. G., Soura, K., Koukouvelas, I. K., & Argyropoulos, N. G. (2017). UAV vs classical aerial photogrammetry for archaeological studies. *Journal of Archaeological Science: Reports*, *14*, 758–773. https://doi.org/10.1016/j.jasrep.2016.09.004

Nilsson, H. (1995). Remote sensing and image analysis in plant pathology. *Annual Review of Phytopathology*, *33*, 489–528. https://doi.org/10.1146/annurev.py.33.090195.002421

Ortega-Terol, D., Hernandez-Lopez, D., Ballesteros, R., & Gonzalez-Aguilera, D. (2017). Automatic hotspot and sun glint detection in UAV multispectral images. *Sensors*, *17*(10), 2352. https://doi.org/10.3390/s17102352

Paone, R., & Rispoli, P. (2011). P. Rispoli e R. Paone, Pompei, Canale Conte Sarno,Lavori di sistemazione e rifunzionalizzazione. *Rivista Di Studi Pompeiani XXII*. Retrieved from https://www.academia.edu/12155319/P_Rispoli_e_R_Paone_Pompei_Canale_Conte_Sarno_Lavori_di_sistemazione_e_rifunzionalizzazione_in_Rivista_di_Studi_Pompeiani_XXII_2011

Parslow, C. (1988). Documents illustrating the excavations of the Praedia of Julia Felix in Pompeii. *Rivista Di Studi Pompeiani : II, 1988*, 37–48. https://doi.org/10.1400/258585

Patrucco, G., Cortese, G., Giulio Tonolo, F., & Spanò, A. (2020). Thermal and optical data fusion supporting built heritage analyses. *The International Archives of the Photogrammetry, Remote Sensing and Spatial Information Sciences*, *XLIII-B3-2020*, 619–626. https://doi.org/10.5194/isprs-archives-XLIII-B3-2020-619-2020

Peña-Villasenín, S., Gil-Docampo, M., & Ortiz-Sanz, J. (2024). Hidden Archaeological remains in heterogeneous vegetation: a crop marks study in fortified settlements of Northwestern Iberian Peninsula. *Remote Sensing*, *16*(21), 3923. https://doi.org/10.3390/rs16213923

Pepe, M., Fregonese, L., & Scaioni, M. (2018). Planning airborne photogrammetry and remote-sensing missions with modern platforms and sensors. *European Journal of Remote Sensing*, *51*(1), 412–436. https://doi.org/10.1080/22797254.2018.1444945

Ronchi, D., Limongiello, M., & Barba, S. (2020). Correlation among earthwork and cropmark anomalies within archaeological landscape investigation by using LiDAR and multispectral technologies from UAV. *Drones*, *4*(4), 72. https://doi.org/10.3390/drones4040072

Salgado Carmona, J. Á., Quirós, E., Mayoral, V., & Charro, C. (2020). Assessing the potential of multispectral and thermal UAV imagery from archaeological sites. A case study from the Iron Age hillfort of Villasviejas del Tamuja (Cáceres, Spain). *Journal of Archaeological Science: Reports*, *31*, 102312. https://doi.org/10.1016/j.jasrep.2020.102312

Sammartano, G., Chiabrando, F., & Spanò, A. (2020). Oblique images and direct photogrammetry with a fixed wing platform: first test and results in Hierapolis of Phrygia (TK). *The International Archives of the Photogrammetry, Remote Sensing and Spatial Information Sciences*, *XLIII-B2-2020*, 75–82. https://doi.org/10.5194/isprs-archives-XLIII-B2-2020-75-2020

Santoro, V., Patrucco, G., Lingua, A., & Spanò, A. (2023). Multispectral UAV data enhancing the knowledge of landscape heritage. *The International Archives of the Photogrammetry, Remote Sensing and Spatial Information Sciences*, *XLVIII-M-2–2023*, 1419–1426. https://doi.org/10.5194/isprs-archives-XLVIII-M-2-2023-1419-2023

Sauerbier, M., & Eisenbeiss, H. (2010). UAVs For the documentation of archaeological excavations. *International Archives of the Photogrammetry, Remote Sensing and Spatial Information Sciences*, *XXXVIII*(5), 526–531. ISPRS. https://doi.org/10.3929/ethz-b-000026303

Schaepman, M. E., Ustin, S. L., Plaza, A. J., Painter, T. H., Verrelst, J., & Liang, S. (2009). Earth system science related imaging spectroscopy—An assessment. *Remote Sensing of Environment*, *113*(Suppl.1), S123–S137. https://doi.org/10.1016/j.rse.2009.03.001

Sonnemann, T. F., Comer, D. C., Patsolic, J. L., Megarry, W. P., Herrera Malatesta, E., & Hofman, C. L. (2017). Semi-automatic detection of indigenous settlement features on hispaniola through remote sensing data. *Geosciences*, *7*(4), 127. https://doi.org/10.3390/geosciences7040127

Spinosa, A. (2022). Restauri, fruizione e ars topiaria nella Regio II di Pompei. In *Edizione degli scavi nei Praedia di Iulia Felix e studi sulla Regio II di Pompei* (pp. 61–73). Pisa, Italy: Pisa University Press. Retrieved from https://www.academia.edu/95674889/A_Anguissola_R_Olivito_PRAEDIA_I_Edizione_degli_scavi_nei_Praedia_di_Iulia_Felix_e_studi_sulla_Regio_II_di_Pompei_Pisa_University_Press_Pisa_2022

Takhtkeshha, N., Mandlburger, G., Remondino, F., & Hyyppä, J. (2024). Multispectral light detection and ranging technology and applications: a review. *Sensors*, *24*(5), 1669. https://doi.org/10.3390/s24051669

Traviglia, A., & Torsello, A. (2017). Landscape pattern detection in archaeological remote sensing. *Geosciences*, *7*(4), 128. https://doi.org/10.3390/geosciences7040128

Urbini, S., Sapia, V., Materni, V., Marchetti, M., Anguissola, A., Taccola, E., & Olivito, R. (2021). *Indagini geofisiche nell'hortus dei Praedia Iuliae Felicis (Pompei, II, 4). Risultati preliminari e prospettive* [PDF]. https://doi.org/10.13131/ARCHEOLOGICADATA-C4V3-E890

Uribe, P., Angás, J., Pérez-Cabello, F., de la Riva, J., Bea, M., Serreta, A., … Martín-Bueno, M. (2015). Aerial mapping and multi-sensors approaches from remote sensing applied to the Roman archaeological heritage. *The International Archives of the Photogrammetry, Remote Sensing and Spatial Information Sciences*, *XL-5-W4*, 461–467. https://doi.org/10.5194/isprsarchives-XL-5-W4-461-2015

Verhoeven, G., Smet, P., Poelman, D., & Vermeulen, F. (2009). Spectral characterization of a digital still camera's NIR modification to enhance archaeological observation. *IEEE Transactions on Geoscience and Remote Sensing*, *47*(10), 3456–3468. https://doi.org/10.1109/TGRS.2009.2021431

Watts, A. C., Ambrosia, V. G., & Hinkley, E. A. (2012). Unmanned aircraft systems in remote sensing and scientific research: classification and considerations of use. *Remote Sensing*, *4*(6), 1671–1692. https://doi.org/10.3390/rs4061671

Yang, H., Wang, S., Wang, S., Zhao, P., Ai, M., & Hu, Q. (2024). Moated site object detection using time series satellite imagery and an improved deep learning model in northeast Thailand. *Journal of Archaeological Science*, *171*, 106070. https://doi.org/10.1016/j.jas.2024.106070

Zanni, S., & De Rosa, A. (2019). Remote Sensing Analyses on Sentinel-2 Images: Looking for Roman Roads in Srem Region (Serbia). *Geosciences*, *9*(1), 25. https://doi.org/10.3390/geosciences9010025

Zhang, D., Hou, L., Lv, L., Qi, H., Sun, H., Zhang, X., … Liao, Y. (2025). Precision agriculture: temporal and spatial modeling of wheat canopy spectral characteristics. *Agriculture*, *15*(3), 326. https://doi.org/10.3390/agriculture15030326

Zhao, Q., & Qu, Y. (2024). The retrieval of ground NDVI (Normalized Difference Vegetation Index) data consistent with remote-sensing observations. *Remote Sensing*, *16*(7), 1212. https://doi.org/10.3390/rs16071212